Astronomy & Astrophysics manuscript no. goods˙vimos2˙141209
December 21, 2009

The Great Observatories Origins Deep Survey

VLT/VIMOS Spectroscopy in the GOODS-South Field: Part II

I. Balestra[1], V. Mainieri[1], P. Popesso[2], M. Dickinson[3], M. Nonino[4], P. Rosati[1], H. Teimoorinia[1,5], E. Vanzella[4], S. Cristiani[4], C. Cesarsky[1], R.A.E. Fosbury[1], H. Kuntschner[1], and A. Rettura[6] the GOODS team

[1] European Southern Observatory, Karl-Schwarzschild-Strasse 2, D-85748 Garching, Germany
[2] Max-Planck-Institut fur extraterrestrische Physik, Giessenbachstrasse 2, 85748 Garching, Germany
[3] National Optical Astronomy Observatory, P.O. Box 26732, Tucson, AZ 85726
[4] INAF - Osservatorio Astronomico di Trieste, Via G.B. Tiepolo 11, 40131 Trieste, Italy
[5] Institute for Advanced Studies in Basic Sciences, P.O. Box 45159-1159, Zanjan 45159, Iran
[6] University of California, 3401 Watkins Drive, Riverside, CA 92521 ⋆ ⋆⋆

Received 2009/ Accepted 2009

ABSTRACT

Context. We present the full data set of the VIsible Multi-Object Spectrograph (VIMOS) spectroscopic campaign of the ESO/GOODS program in the Chandra Deep Field South (CDFS), which complements the FORS2 ESO/GOODS spectroscopic campaign.
Aims. The ESO/GOODS spectroscopic programs are aimed at reaching signal-to-noise ratios adequate to measure redshifts for galaxies with AB magnitudes in the range $\sim 24-25$ in the B and R band using VIMOS, and in the z band using FORS2.
Methods. The GOODS/VIMOS spectroscopic campaign is structured in two separate surveys using two different VIMOS grisms. The VIMOS Low Resolution Blue (LR-Blue) and Medium Resolution (MR) orange grisms have been used to cover different redshift ranges. The LR-Blue campaign is aimed at observing galaxies mainly at $1.8 < z < 3.5$, while the MR campaign mainly aims at galaxies at $z < 1$ and Lyman Break Galaxies (LBGs) at $z > 3.5$.
Results. The full GOODS/VIMOS spectroscopic campaign consists of 20 VIMOS masks. This release adds 8 new masks to the previous release (12 masks, Popesso et al. 2009). In total we obtained 5052 spectra, 3634 from the 10 LR-Blue masks and 1418 from the 10 MR masks. A significant fraction of the extracted spectra comes from serendipitously observed sources: $\sim 21\%$ in the LR-Blue and $\sim 16\%$ in the MR masks. We obtained 2242 redshifts in the LR-Blue campaign and 976 in the MR campaign for a total success rate of 62% and 69% respectively, which increases to 66% and 73% if only primary targets are considered. The typical redshift uncertainty is estimated to be $\sigma_z \simeq 0.0012$ ($\sim 255\,\mathrm{km\,s^{-1}}$) for the LR-Blue grism and $\sigma_z \simeq 0.00040$ ($\sim 120\,\mathrm{km\,s^{-1}}$) for the MR grism. By complementing our VIMOS spectroscopic catalog with all existing spectroscopic redshifts publicly available in the CDFS, we compiled a redshift master catalog with 7332 entries, which we used to investigate large scale structures out to $z \simeq 3.7$. We produced stacked spectra of LBGs in a few bins of equivalent width (EW) of the Ly-α and found evidence for a lack of bright LBGs with high EW of the Ly-α. Finally, we obtained new redshifts for 12 X-ray sources of the CDFS and extended-CDFS.
Conclusions. After the completion of the two complementary ESO/GOODS spectroscopic campaigns with VIMOS and FORS2 at VLT, the number of spectroscopic redshifts in CDFS/GOODS field increased dramatically, in particular at $z \gtrsim 2$. These data provide the redshift information indispensable to achieve the scientific goals of GOODS, such as tracing the evolution of galaxy masses, morphologies, clustering, and star formation.

Key words. Cosmology: observations – Cosmology: deep redshift survey – Cosmology: large scale structure of the universe – Galaxies: evolution

1. Introduction

The Great Observatories Origins Deep Survey (GOODS) is a public, multi-facility project aimed at gathering the best and deepest multi-wavelenght data to investigate some of the most profound cosmological issues, such as the formation and evolution of galaxies and active galactic nuclei, the distribution of luminous and dark matter at high redshift, the cosmological parameters from distant supernovae, and the extragalctic background light (for an overview of GOODS, see Dickinson et al. 2003; Renzini et al. 2003; Giavalisco et al. 2004). The program has targeted two carefully selected fields, the Hubble Deep Field North (HDFN) and the Chandra Deep Field South (CDFS), with three NASA Great Observatories (HST, Spitzer and Chandra), ESA's XMM-Newton, and a wide variety of ground-based facilities. The area common to all the observing programs is 320 arcmin^2, equally divided between the North and South fields.

Spectroscopy is crucial to reach the scientific goals of GOODS. In order to reconstruct the evolutionary history of galaxy masses, morphologies, clustering, or star formation, reliable redshifts are essential. Consequently, the CDFS has been target of several spectroscopic campaigns over the last decade (Cristiani et al. 2000; Croom et al. 2001; Cimatti et al. 2002; Bunker et al. 2003; Stanway et al. 2004; Strolger et al. 2004; van

Send offprint requests to: I. Balestra, e-mail: ibalestr@eso.org

⋆ Based on observations made at the European Southern Observatory, Paranal, Chile (ESO program 171.A-3045 *The Great Observatories Origins Deep Survey: ESO Public Observations of the SIRTF Legacy/HST Treasury/Chandra Deep Field South*.)

⋆⋆ Catalogs and data products are available in electronic form at http://archive.eso.org/cms/eso-data/data-packages

der Wel et al. 2004; Dickinson et al. 2004; Szokoly et al. 2004; Le Fèvre et al. 2005; Mignoli et al. 2005; Vanzella et al. 2005, 2006; Ravikumar et al. 2007; Vanzella et al. 2008; Popesso et al. 2009).

The ESO/GOODS spectroscopic program was designed to observe galaxies for which VLT optical spectroscopy was likely to obtain useful data. The program was organized into two large campaigns, carried out with the FOcal Reducer and low dispersion Spectrograph (FORS2) at VLT/UT1 and with the VIsible Multi-Object Spectrograph (VIMOS) at VLT/UT3. The ESO/GOODS spectroscopic program made full use of the VLT instrument capabilities, matching targets to instrument and disperser combinations in order to maximize the effectiveness of the observations.

The FORS2 campaign is completed (Vanzella et al. 2005, 2006, 2008). As a result, 1715 spectra of 1225 individual targets were observed and 887 redshifts were determined with a typical uncertainty of $\sigma_z \simeq 0.001$. Galaxies were selected adopting three different color criteria and using photometric redshifts. The resulting redshift distribution spans two redshift domains: from $z = 0.5$ to 2 and from $z = 3$ to 6.5. The reduced spectra and the derived redshifts were released to the community through the ESO web pages `http://archive.eso.org/cms/eso-data/data-packages`.

The GOODS/VIMOS spectroscopic survey complements the FORS2 survey in terms of completeness and sky coverage. The FORS2 campaign was designed to take advantage of the instrument's very high throughput at red wavelengths, which allows detecting rest-frame optical and near-ultraviolet spectral features (such as the [OII]3727 Å emission line) out to $z \simeq 1.6$, and rest-frame UV emission and absorption lines at $z > 4$. On the other hand, the VIMOS campaign takes advantage of VIMOS's very large field of view, multiplexing capability, and good instrumental throughput at roughly 3600-9000 Å, which enable measuring large numbers of redshifts at $z < 1.4$ from the [OII]3727 Å emission line and other optical and near-UV features, as well as redshifts between 1.5 and 3.5 from Lyman-α emission and rest-frame UV absorption lines. The cumulative source counts on the CDFS taken from the deep public FORS1 data (Szokoly et al. 2004), show that down to $V_{AB} = 25$ mag there are ~ 6000 objects over the 160 arcmin^2 of the GOODS-S field. Only the high multiplexing capabilities of VIMOS at VLT could ensure to reach the required completeness in a reasonable amount of time.

The GOODS/VIMOS program used two different observational configurations, with different object selection criteria. Observations with the Medium Resolution (MR) orange grism target galaxies in the redshift ranges $0.5 < z < 1.3$ (primarily from [OII]) and $z > 3.5$ (from Ly-α). Observations with the Low Resolution Blue (LR-Blue) grism cover the wavelengths of Ly-α and UV rest-frame absorption lines at $1.8 < z < 3.5$, a range not covered by the FORS2 spectroscopy. On average, ~330 objects per mask have been observed with the low resolution ($R \simeq 180$) blue grism and ~140 with the medium resolution ($R \simeq 580$) orange grism. The overall goal of the GOODS spectroscopic campaign was to reach signal-to-noise (S/N) ratios adequate to measure redshifts for galaxies with AB magnitudes in the range $\sim 24 - 25$, in the B band for objects observed with the VIMOS LR-Blue grism, in the R band for objects observed with the VIMOS MR grism, and in the z band for objects observed with FORS2.

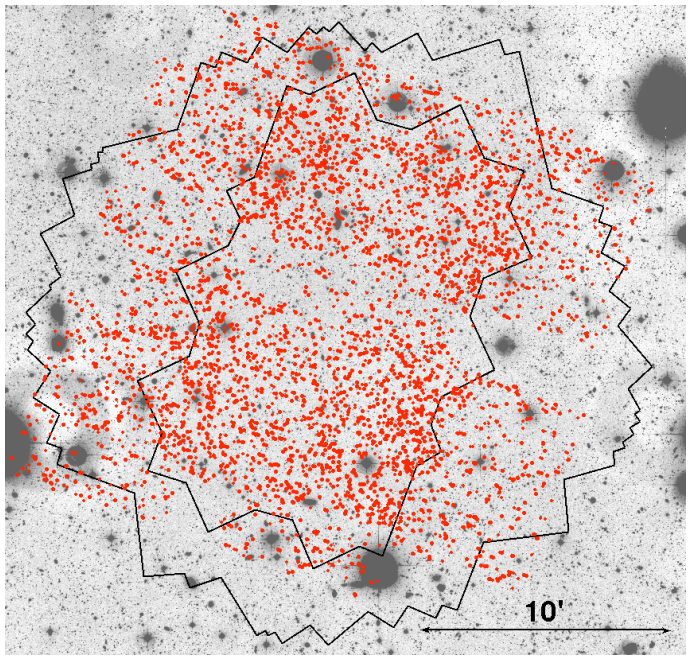

Fig. 1. Spatial distribution of objects from the whole (LR-Blue plus MR grism) GOODS/VIMOS spectroscopic campaign (*red circles*) over the ESO-WFI R-band image. The contours outline the area of the 2 Ms exposure of the CDFS and the GOODS-S field.

The first part of the GOODS/VIMOS spectroscopic survey has been recently released (Popesso et al. 2009, hereafter P09). The first release includes 2344 spectra from 6 LR-Blue masks and 968 from 6 MR masks. The number of redshifts obtained is 1481 and 656 for the LR-Blue and the MR campaign, respectively.

In this paper we report on the full data set of the VIMOS spectroscopic follow-up campaign in the CDFS, carried out with the VIMOS instrument at the VLT from ESO observing periods P74 through P78 (mid 2004 through early 2007). This final release includes a total of 10 masks for the LR-Blue grism and 10 masks for the MR grism.

The plan of the paper is as follows. In Sect. 2 we describe the GOODS/VIMOS survey and the target selection criteria used. In Sect. 3 we describe the observations and the data reduction. The redshift determination and the full data set is presented in Sect. 4 and discussed in Sect. 5. In Sect. 6 we summarize the results of the GOODS/VIMOS spectroscopic campaign and our conclusions.

Throughout this paper the magnitudes are given in the AB system (AB $\equiv 31.4 - 2.5 \log\langle f_\nu/\mathrm{nJy}\rangle$), and the ACS F435W, F606W, F775W, and F850LP filters are denoted hereafter as B_{435}, V_{606}, i_{775} and z_{850}, respectively. We assume a cosmology with $\Omega_{\rm tot}, \Omega_M, \Omega_\Lambda = 1.0, 0.3, 0.7$ and $H_0 = 70$ km s^{-1} Mpc^{-1}.

2. Target selection

VIMOS (LeFevre et al. 2003) is a 4-channel imaging spectrograph, each channel ("quandrant") covering $\sim 7 \times 8$ arcmin^2 for a total field of view ("pointing") of ~ 218 arcmin^2. Because of its geometry (a $16' \times 18'$ field of view, with a cross gap of $2'$ between the quadrants) only $\sim 50\%$ of VIMOS field of view overlaps with the $10' \times 16'$ area roughly defining the GOODS-S field. The spectroscopic campaign was designed to cover the whole GOODS area. At least 3 VIMOS pointing are required

to cover the GOODS area, filling the gaps between the quadrants, with some fraction of the VIMOS coverage extending outside the GOODS-S field into the CDFS and the "Extended" CDFS (ECDFS). Figure 1 shows the spatial distribution of the sources observed in the two VIMOS surveys (both LR-Blue and MR objects), which outlines the VIMOS coverage of the GOODS/CDFS field.

The survey strategy and target-selection criteria are the same as in P09, where a detailed description can be found. Here, we recall the imaging data, the source catalogs, and the main criteria used for target selection in the GOODS/VIMOS spectroscopic campaign. The imaging data and source catalogs used are:

- CTIO 4 m MOSAIC U-band imaging and ESO 2.2 m WFI B- and R-band imaging, covering the $30' \times 30'$ ECDFS, with AB magnitude 5σ depths 26, 26.2 and 25.8 mag, respectively (Giavalisco et al. 2004), used for Lyman break U-dropout and "sub-U-dropout" color selection, both inside and outside the nominal GOODS-S area;
- HST-ACS B_{435} and z_{850} imaging, covering the GOODS-South field ($\sim$ 165 arcmin^2) with depth 27.8 and 27.4 mag (Giavalisco et al. 2004), used for the BzK color-selection technique within the GOODS-S field;
- VLT-ISAAC K_s-band imaging covering the GOODS-S field with depth 25.1 mag (Retzlaff et al. in preparation), for applying the BzK selection technique in GOODS-S field;
- CDFS X-ray catalog (Giacconi et al. 2002; Lehmer et al. 2005), covering an area larger than GOODS-S, down to an on-axis flux limit of approximately 5×10^{-17} erg cm^2 s^{-1} in the 0.5 – 2 keV band.

The wavelength range covered by the VIMOS LR-Blue grism (3500-6900 Å) is suitable for the detection of ultraviolet absorption and emission features of objects in the redshift range $1.8 < z < 3.8$. Targets for the VIMOS LR-Blue grism were selected using the following criteria:

- U-dropouts, i.e. Lyman-break color-selection of galaxies, using the CTIO U and WFI B and R photometry, designed to select blue, star-forming galaxies at $z \approx 3$;
- so-called "sub-U-dropouts", i.e. UBR color-selected objects with $U - B$ colors somewhat bluer than those of the 'normal' $z \sim 3$ U-dropout Lyman break selection criteria, designed to select star-forming galaxies at somewhat lower redshifts than those of the regular U-dropouts, nominally $z \approx 1.8$ to 2.5;
- BzK color-selection (Daddi et al. 2004), designed to select galaxies at $1.4 < z < 2.5$. Late in the VIMOS campaign, additional Spitzer/IRAC color criteria were applied to try to refine the BzK method (see P09);
- X-ray sources from the CDFS and the ECDFS X-ray catalogs (Giacconi et al. 2002; Lehmer et al. 2005).

No low redshift galaxies were intentionally targeted for the LR-Blue masks, although as discussed in P09, some foreground interlopers do "contaminate" the color-selected samples, particularly the sub-U-dropouts. A magnitude cut at $B < 24.5$ mag was applied to all target catalogs listed above.

The wavelength range of the VIMOS MR grism is 4000-10000 Å, similar to that of FORS2. However, because of the stronger fringing at red wavelength ($\lambda \geq 7000$ Å) and the lower red throughput of VIMOS compared to FORS2, optical rest-frame spectral features for galaxies at $z > 1$ and ultraviolet rest-frame spectral features of Lyman break galaxies (LBGs) at $z \gtrsim 4.8$ are harder to detect with VIMOS than with FORS2. Therefore, the target selection for the VIMOS MR grism was limited to brighter galaxies (mainly expected to be at $z < 1.2$), and to color-selected LBGs in the redshift range $2.8 < z < 4.8$. Target selection for the MR grism used the available imaging data and photometry catalogs according to the following criteria:

- galaxies with $R < 24.5$, with no other color pre-selection, excluding VIMOS LR-Blue targets and objects already observed in other spectroscopic programs. In the later VIMOS campaigns, some preference was given to galaxies detected at 24 μm from the GOODS Spitzer MIPS data (Dickinson et al. in preparation; Chary et al. in preparation), meeting the same $R < 24.5$ mag limit.
- relatively bright Lyman break galaxies at $i_{775} < 25$, selected as B_{435}, V_{606} dropouts (nominally, redshifts $z \approx 4$ and 5, respectively), according to the same color criteria described in Vanzella et al. (2005, 2006, 2008).

No photometric redshifts were used, nor a surface brightness selection was applied when selecting galaxies for observations. GOODS/VIMOS masks were designed to avoid as much as possible objects already observed in previous redshift surveys (e.g. Cimatti et al. 2002; Szokoly et al. 2004; Le Fèvre et al. 2005; Vanzella et al. 2005, 2006, 2008).

3. Observations and data reduction

The VLT/VIMOS spectroscopic observations were carried out in service mode during ESO observing periods P74-P78. A log of all the GOODS/VIMOS observations is presented in Table 1. The total exposure time per mask is 4 h. Each LR-Blue mask consists of 10 exposures of 24 min, while each MR mask consists of 12 exposures of 20 min. This work adds 8 new masks to the previous release (12 masks, P09), for a total of 20 VIMOS masks. All the masks were designed with 1″ slits. The spatial scale for VIMOS is 0.205″/pixel.

In the LR-Blue campaign, the LR-Blue grism was used together with the Order Sorting OS_Blue cutoff filter. In this configuration the useful wavelength range is 3700 – 6700 Å, the nominal resolution is $R = \lambda/\Delta\lambda = 180$, corresponding to a spectral resolution of $\sim$ 28 Å, and the dispersion is 5.7 Å/pixel.

The MR grism and the GG475 filter were used in the MR campaign. In this configuration the useful wavelength range is 4800 – 10000 Å, the nominal resolution is $R = \lambda/\Delta\lambda = 580$, which corresponds to a spectral resolution of $\sim$ 13 Å, and the dispersion is 2.55 Å/pixel.

For a detailed description of the preparation of VIMOS observations and the procedure used for data reduction we refer the reader to P09.

3.1. Target coordinates

The pipeline processing of the GOODS/VIMOS data was carried out using the VIMOS Interactive Pipeline Graphical Interface (VIPGI, Scodeggio et al. 2005). As it was pointed out in the previuos release (P09), since the rotation angle of the GOODS/VIMOS pointings (−20 deg) is different from the default values accepted by VIPGI (0 or 90 deg), the software does not provide the astrometry for the extracted spectra. We followed the same procedure described in P09 to retrieve target coordinates. In addition, we cross-correlated the "reconstructed" coordinates, obtained as in P09, with the WFI R-band catalog. In our final released catalogs we provide for each object both the

Table 1. Log of VIMOS observations for the entire GOODS/VIMOS spectroscopic campaigns. Columns list the following information: (1) GOODS/VIMOS mask identification number, (2) date of the observations, and (3) number of exposures per mask times duration of single exposure.

Mask ID	Date	Exp. time (s)
(1)	(2)	(3)
LR-Blue masks (P09)		
GOODS_LRb_001	Sept.-Oct. 2004	10×1440
GOODS_LRb_001_1	Nov. 2004	10×1440
GOODS_LRb_002	Oct.-Nov. 2004	10×1440
GOODS_LRb_003_new	Oct. 2005	10×1440
GOODS_LRb_003_new_1	Oct.-Nov. 2005	10×1440
GOODS_LRb_003_new_2	Nov.-Dec. 2005	10×1440
MR masks (P09)		
GOODS_MR_001	Nov. 2004	12×1200
GOODS_MR_002_1	Jan. 2005	12×1200
GOODS_MR_new_1	Dec. 2005	12×1200
GOODS_MR_new_2	Jan. 2006	12×1200
GOODS_MR_new_2_1	Jan. 2006	12×1200
GOODS_MR_new_3_c	Sept.-Oct. 2006	12×1200
LR-Blue masks (this work)		
GOODS_LRb_002_1	Dec. 2004	10×1440
GOODS_LRb_dec06_1	Nov. 2006	10×1440
GOODS_LRb_dec06_2	Nov. 2006	10×1440
GOODS_LRb_dec06_3	Nov.-Dec. 2006	10×1440
MR masks (this work)		
GOODS_MR_dec06_1	Oct. 2006	12×1200
GOODS_MR_dec06_2	Oct.-Nov. 2006	12×1200
GOODS_MR_dec06_3	Oct. 2006	12×1200
GOODS_MR_dec06_4	Jan. 2007	12×1200

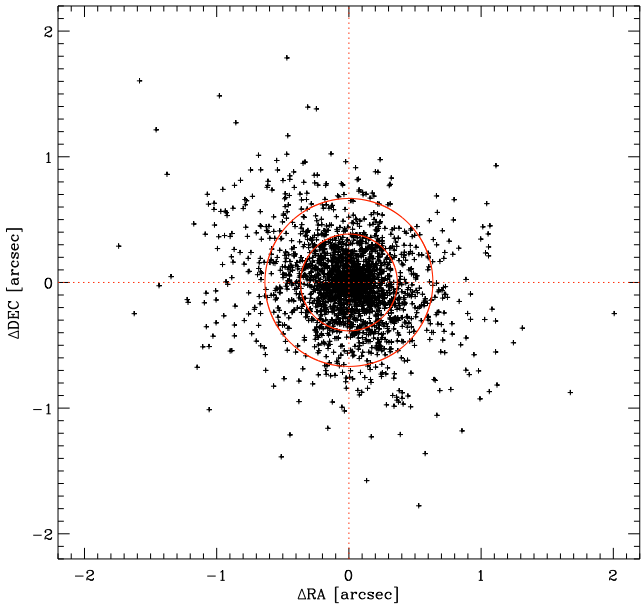

Fig. 2. ΔRA–ΔDEC distribution computed between VIMOS "reconstructed" coordinates and WFI coordinates of matching WFI *R*-band object for the VIMOS LR-Blue spectroscopic catalog. The rms dispersion is about 0.2″ on both axes. We display two regions encircling 68% and 90% of the objects, which have radii of 0.307″ and 0.635″, respectively.

"reconstructed" VIMOS coordinates and the coordinates of the matching (within a positional tolerance of 1″) WFI *R*-band object. If no match is found, we repeat the "reconstructed" VIMOS coordinates. Fig. 2 shows the distribution of ΔRA and ΔDEC computed between VIMOS "reconstructed" coordinates and the coordinates of the matching WFI *R*-band object for the VIMOS LR-Blue spectroscopic catalog. The rms dispersion is smaller than 0.3″ on both coordinates ensuring accurate target identification.

It is worth noticing that 48 cases (39 in the LR-Blue and 9 in the MR grism) could be identified, where two closely separated ($\lesssim$ 1″) spectra are extracted in the same slit for two objects that are blended in WFI images and, therefore, match a single WFI object. In all these cases, the WFI coordinates and the coordinate-based names assigned to each pair are the same. However, the information on the "correct" position may still be retrieved from their reconstructed VIMOS coordinates. In Fig. 3 we show one such case. The comparison between the WFI *R*-band and the ACS *z*-band images clearly reveals the close pair of sources and the good accuracy of their VIMOS reconstructed position.

As mentioned in P09, due to a bug, VIPGI assigns wrong focal plane coordinates to a small number of objects in slits with more than 2 spectra. In most cases the extracted spectra of these objects lie very close to the edge of the 2D spectrum. Targets with uncertain coordinates were 81 in the LR-Blue campaign (out of which 80% had no redshift determination) and 34 in the MR campaign (50% without redshift), all of which are serendipitously observed objects. Among them, we selected objects having a redshift determination (18 in the LR-Blue catalog and 16 in the MR catalog), in order to attempt to retrieve their coordinates manually. From a visual inspection of the 2D spectrum and using the coordinates of primary targets and, if present, other objects in the same slit as a reference, we could unambigously identify and retrieve coordinates for all of the 34 objects selected. Their new coordinates are included in the final released catalogs.

The remaining 63 and 18 (from the LR-Blue and the MR catalog respectively) serendipitous objects having uncertain coordinates and no redshift estimate were removed from the final released catalogs.

4. Redshift determination

The total number of GOODS/VIMOS spectra extracted is 3634 in the LR-Blue and 1418 in the MR campaign. We were able to determine 2242 and 976 redshifts in the LR-Blue and the MR campaign, respectively. Serendipitous objects constitute ∼ 21% of the LR-Blue and ∼ 16% of the MR objects. We have identified 3305 single LR-Blue objects and 1297 single MR objects. Out of those, we were able to determine 2074 and 885 redshifts in the LR-Blue and the MR campaign, respectively.

The redshifts were estimated following a different procedure compared to P09. We avoid the use of the *rvsao* package in IRAF to cross-correlate individually observed spectra with template spectra. Instead, we proceed via visual inspection first, assigning redshifts only to the most obvious cases, where more than 2 spectral features could be unambigously identified. VIPGI's software *EZ* was subsequently used for the cross-correlation with template spectra (i.e. ordinary S0, Sa, Sb, Sc, and elliptical galaxies at low redshift, Lyman break galaxies and quasars at high redshift) in dubious cases only.

Redshift were determined through the identification of prominent features of galaxy spectra:

– at low redshift the absorption features: the 4000 Å break, Ca H and K, Hδ and Hβ in absorption, G-band, MgII 2798

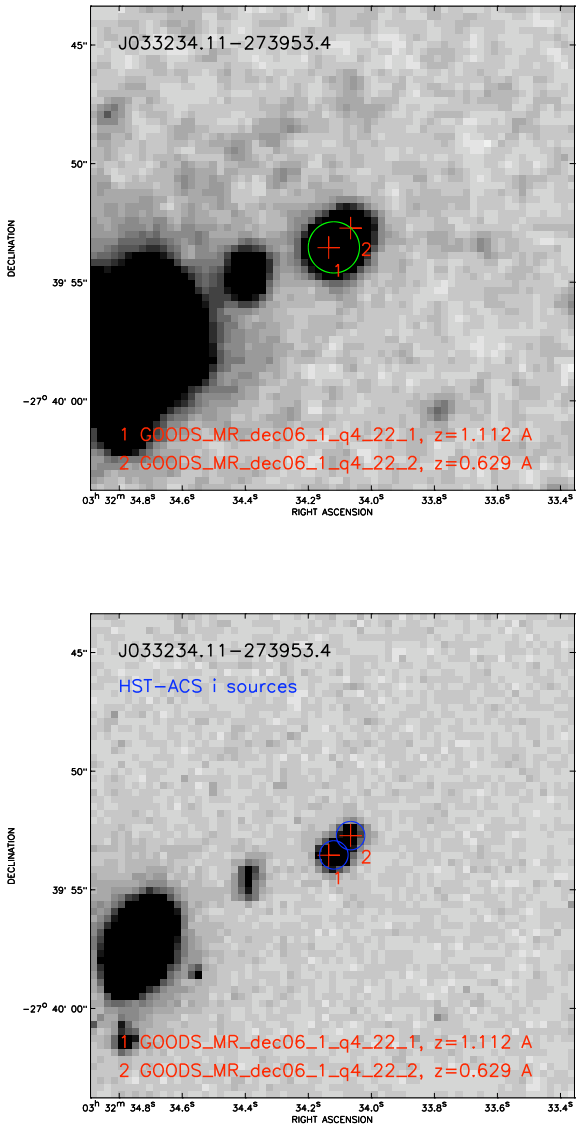

Fig. 3. WFI *R*-band (*upper panel*) and ACS *z*-band (*lower panel*) $20'' \times 20''$ cutout centered on J033234.11-273953.4. Red crosses display the reconstructed VIMOS coordinates of the two objects in slit. The position of the WFI-matched object is shown in green and the position of the two corresponding ACS *i*-band sources are shown in blue.

- and the emission features: [O II]3727, [O III]5007, Hβ, Hα
- at high redshift: Lyα, in emission and absorption, ultraviolet absorption features such as [Si II]1260, [O I]1302, [C II]1335, [Si IV]1393,1402, [S II]1526, [C IV]1548,1550, [Fe II]1608 and [Al III]1670

In analogy to the complementary GOODS/FORS2 redshift campaign (Vanzella et al. 2005, 2006, 2008), we use four quality flags to indicate the quality of a redshift estimate. Quality flags are assigned with the following criteria:

- flag A, high quality, i.e. several emission lines and strong absorption features are well identified;
- flag B, intermediate quality, i.e. at least two spectral features are well identified, for instance one emission line plus few absorption features;
- flag C, low quality, i.e. spectral features, either in emission or in absorption, are less clearly identified;
- flag X, no redshift estimated. No features identified.

Each spectrum with the superposed main spectral features, is visually inspected independently by different people and the redshift determination and the quality flag assignment are eventually further refined. On average, each spectrum is checked more than three times. Fig. 4 shows the quality of VIMOS spectra ranked by S/N: typical LR-Blue and MR spectra for quality-A, -B, and -C redshift etimates are shown for comparison.

In $\sim 15\%$ of the cases the redshift is based only on one emission line, usually identified with [O II]3727 or Ly-α. In these cases the continuum shape, the presence of breaks, the absence of other spectral features in the observed spectral range and the broad band photometry are particularly important in the evaluation. In general these solo-emission line redshifts are classified as "likely" (B) or "tentative" (C) if no other information is provided by the continuum.

In order to investigate possible differences in the redshift estimates that could be introduced by the different methods utilized in the two releases, we compared the reshift resulting from the two different methods for two quadrants of one of the new LR-Blue masks. We verified that our procedure produced equivalent results to that used in the previous release, with the only noticeable exception of the absence of an overabundance of low-quality estimates in the range $1.8 \lesssim z \lesssim 2.2$, that was affecting the previous release (see P09; see also Sect.4.1 and Figure 8) and which was probably due to the different method used in determining redshifts.

We estimated the internal redshift accuracy by comparing the redshift measurements of all the objects observed twice in independent VIMOS masks. We found 118 such objects in the LR-Blue masks and 83 in the MR masks with redshift quality flag A or B. In Figure 5 we plot histograms of the difference in redshift measurements ($\Delta z = z_1 - z_2$) separately for the LR-Blue and MR grisms. The difference of redshift measurements in the LR-Blue campaign has a Gaussian distribution with $< \Delta z >= 5.9 \times 10^{-5}$ and $\sigma_{\Delta z} = 0.00120$, therefore the accuracy of single redshift measurements is $\sigma_z = \sigma_{\Delta z}/\sqrt{2} = 0.00084$ ($\sim 255\,\mathrm{km\,s^{-1}}$). For the MR redshifts the Gaussian distribution has a mean $< \Delta z >= 1.2 \times 10^{-4}$ and a dispersion $\sigma_{\Delta z} = 0.00056$, therefore the accuracy on a single measurement is $\sigma_z = 0.00040$ ($\sim 120\,\mathrm{km\,s^{-1}}$).

4.1. Reliabilty of redshifts

In order to assess the reliability of our redshift estimates we compared them with independent measurements from other publicly available spectroscopic surveys in the CDFS: the GOODS-FORS2 campaign (Vanzella et al. 2005, 2006, 2008), the K20 survey (Mignoli et al. 2005), the Szokoly et al. (2004) survey, the VVDS survey (Le Fèvre et al. 2005), and the IMAGES survey (Ravikumar et al. 2007). As in P09, we combined the redshift information from all these surveys into a "master catalog"[1], cleaned from duplicate observations (in case of double or multiple observations we kept the mean value of the redshift estimates). However, to refine the test on redshift reliability performed in P09, we created a "secure" redshift reference sample by selecting only the best-quality (all reliable at > 99% c.l.) redshift determinations for each survey (i.e. GOODS-FORS2 qual-

[1] Available in electronic form at: *http://w4/sci/activities/projects/goods/*

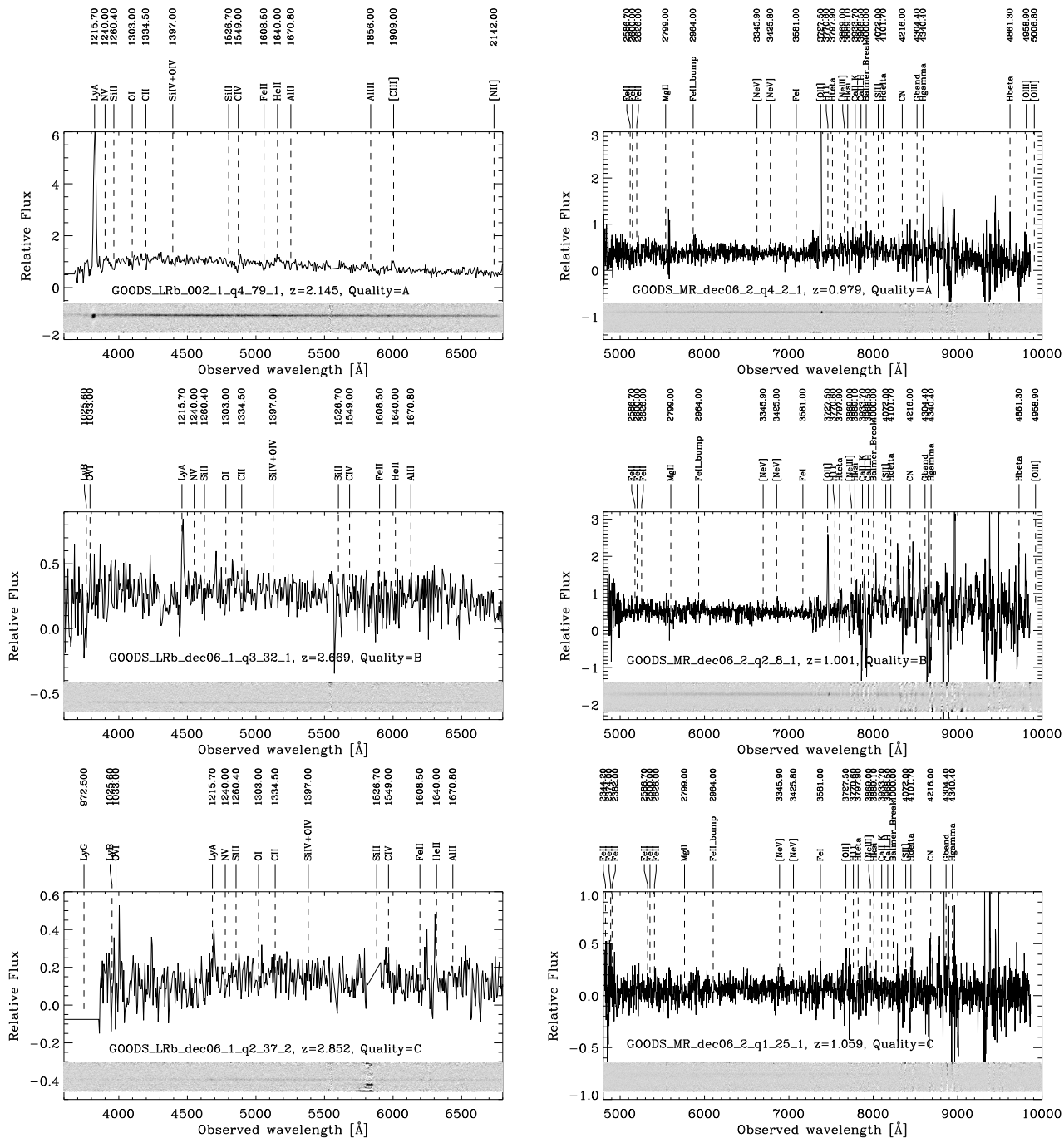

Fig. 4. Examples of VIMOS spectra (unsmoothed) ranked by quality of the redshift estimate. The *left column* shows 1D and 2D spectra obtained with the LR-Blue grism for objects with quality-A, -B, and -C redshift. The *right column* shows the same for the MR grism.

ity A, K20 quality 1, VVDS quality 4, Szokoly et al. (2004) quality 3, and IMAGES quality 2 redshifts).

We found 95 VIMOS LR-Blue targets matching with objects of the high-quality reference sample within a spatial accuracy of 0.3 arcsec or better. Out of them, 21 have VIMOS quality flag A, 19 have flag B, 27 have flag C and 28 do not have a redshift estimate (flag X). Most of the objects without redshift lie in a redshift range not accessible to the LR-Blue grism (i.e. $0.8 < z < 1.7$). "Catastrophic" discrepancies ($|z_{VIMOS} - z_{Others}| > 0.015$) are found only for VIMOS lower-quality redshifts (i.e. flag B and C), which are always less convincing than the corresponding estimates from other surveys. The resulting confidence level is > 99.99% for quality-A (all of the 21 redshifts compared with the reference catalog are correct), ~ 63% for quality-B (7 discrepancies out of 19 compared redshifts), and ~ 19% for quality-C (22 discrepancies out of 27) redshift determinations.

In the VIMOS MR survey we found 78 objects in common with the high-quality reference sample, matching within a spatial accuracy of 0.3 arcsec. Out of them, 10 have VIMOS quality flag A, 35 have quality flag B, 13 have quality flag C, and 20 have no redshift estimate (flag X). We only find 7 catastrophic discrepancies ($|z_{VIMOS} - z_{Others}| > 0.015$): 2 have flag B and 5 have flag C. Hence, we estimate a confidence level of > 99.99% for quality-A (all of the 10 redshifts compared with the reference catalog are correct), ~ 94% for quality B (2 discrepancies out of

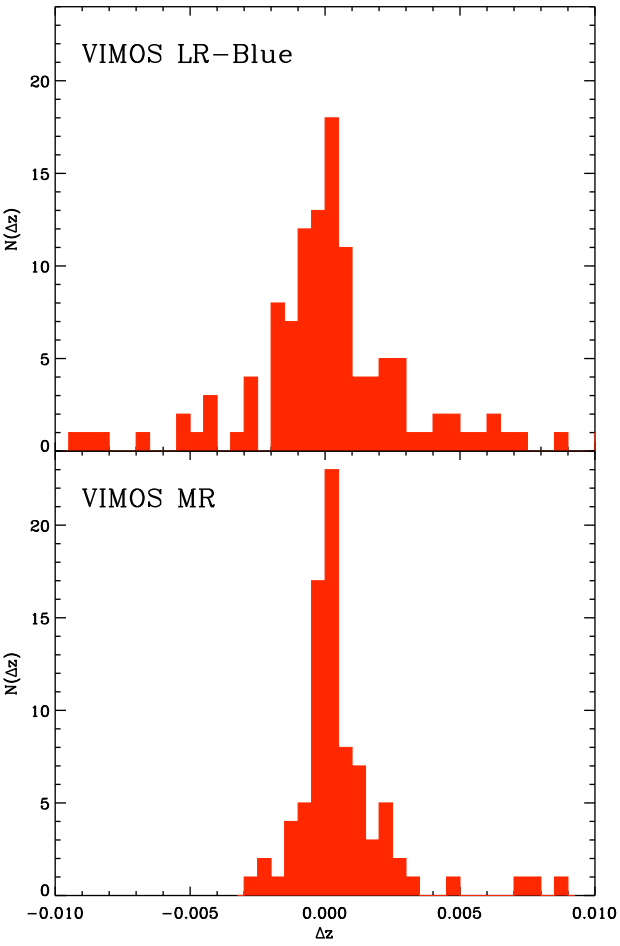

Fig. 5. Redshift differences between objects observed twice or more in independent VIMOS masks. The distribution for the LR-Blue masks (*upper panel*) has a Gaussian distribution with $\sigma_{\Delta z} = 0.00120$, therefore the accuracy on single redshift measurements is $\sigma_z = \sigma_{\Delta z}/\sqrt{2} = 0.00084$ ($\sim 255\,\mathrm{km\,s^{-1}}$), while for the MR masks (*lower panel*) $\sigma_{\Delta z} = 0.00056$ and hence $\sigma_z = 0.00040$ ($\sim 120\,\mathrm{km\,s^{-1}}$).

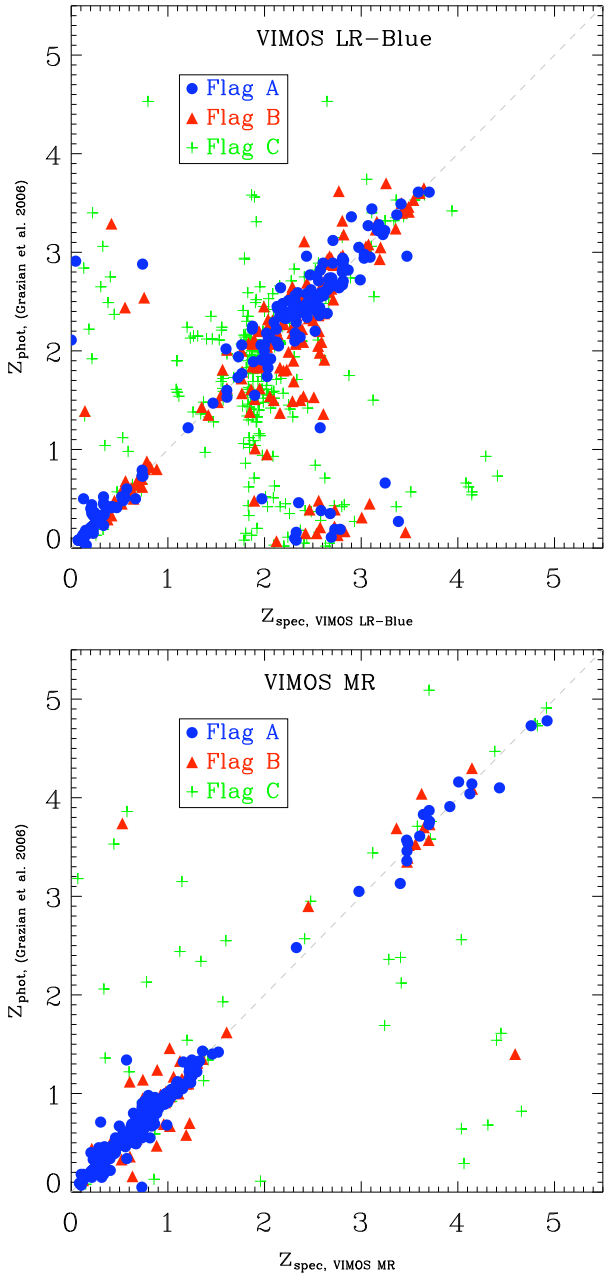

Fig. 6. Photometric redshift (z_{phot} from Grazian et al. 2006) versus spectroscopic redshift (z_{spec}) of the VIMOS LR-Blue (*upper panel*) and VIMOS MR campaign (*lower panel*) for objects with quality flag A (blue circles), B (red triangles), and C (green crosses). The cross-correlation is limited to coordinates matching within 0.3″, i.e. a total of 645 and 523 objects for the LR-Blue and MR, respectively.

35), and 62% for quality C (5 discrepancies out of 13) redshift determinations.

Our new estimates of confidence levels for the reliability of different quality flags are consistent with those obtained in the previous release (see P09) with the only exception of LR-Blue quality-C redshift, which are found to be less reliable then previously estimated.

P09 used also another test to quantify the reliability of the redshifts based on the simultaneous use of two independent photometric catalogs (i.e. Grazian et al. 2006, Daddi et al., private communication). However, results were in line with those obtained from the comparison with high-quality spectroscopic redshift from other surveys. Here, we plot in Figure 6 the comparison between the GOODS/VIMOS spectroscopic redshifts and the GOODS-MUSIC photometric redshifts, which includes all the objects matching within an angular tolerance of 0.3″. In the case of LR-Blue objects, we notice that a few objects, including 16 objects with secure spectroscopic redshifts (i.e. flag A), have large discrepancies compared to their photometric estimates (see also Figure 6 in P09). We checked the spectra of the 13 objects at $2 \lesssim z \lesssim 3.5$ with quality-A spectroscopic redshifts and large discrepancies ($z_{spec} - z_{phot} > 1$) compared to the photometric redshifts. The average WFI R magnitude of these objects is 24.4 and all the spectra have a relatively good S/N, enabling the clear identification of Ly-α in emission or absorption and several UV absorption lines. The spectra of these galaxies have also been used to produce the stacked spectra described in Sect. 5.3.

4.2. Success rate for VIMOS LR-Blue targets

We measured redshifts for 66% (62% including also the secondary serendipitous objects) of the observed LR-Blue spectra. If only high-quality redshift determinations (i.e. A or B) are considered, the success rate of the LR-Blue survey is 43% for the original target sample and 38%, if also secondary targets are

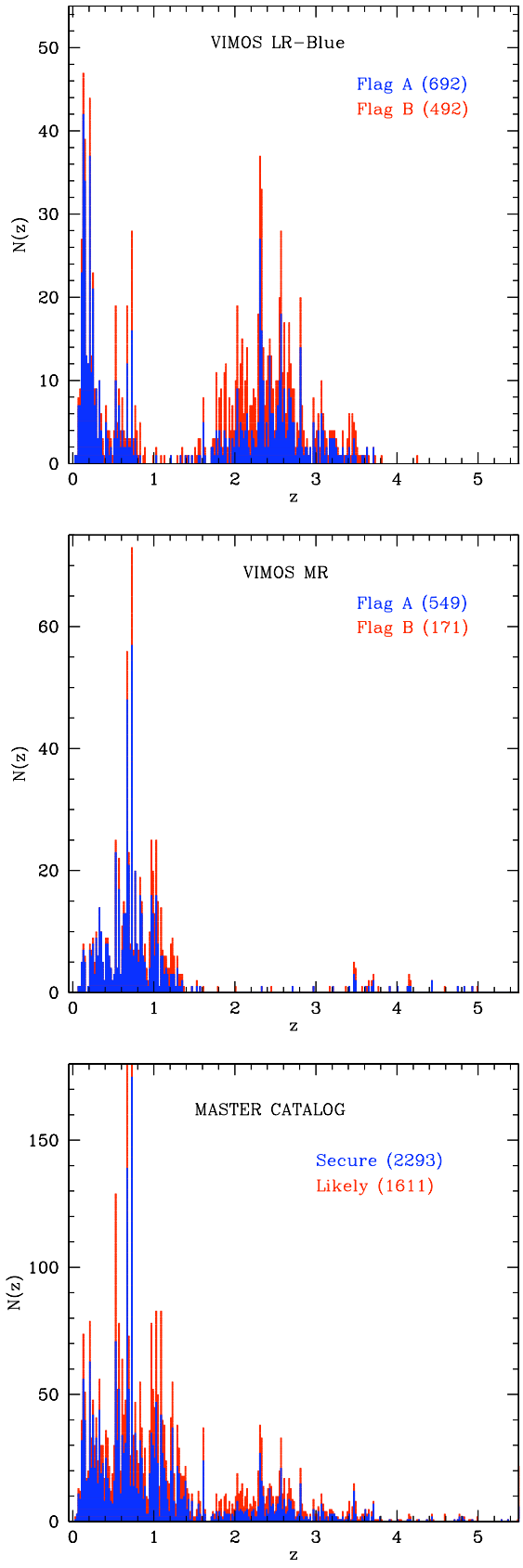

Fig. 7. Redshift distribution of the VIMOS LR-Blue survey (*upper panel*), VIMOS MR survey (*mid panel*), and master compilation of redshifts from independent surveys in the CDFS (*lower panel*). Redshifts of the master compilation were subdivided into "secure" and "likely" as explained in the text (see Sect. 5.1). In the 3 histograms the size of the redshift bin is 0.02. Stars are not plotted.

Table 2. Statistics of the GOODS/VIMOS LR-Blue campaign.

	LR-Blue				
P09* (6 masks)	**A**	**B**	**C**	**X**	**Total**
Num. of entries	617	302	550	810	2279
Primary targets	544	265	415	526	1750
Secondary targets	73	37	135	284	529
This work (4 masks)					
Num. of entries	236	240	297	582	1355
Primary targets	213	208	244	466	1131
Secondary targets	23	32	53	116	224
Total (10 masks)					
Num. of entries	853	542	847	1392	3634
Primary targets	757	473	659	992	2881
Secondary targets	96	69	188	400	753

* For the first release (P09) the numbers of redshifts reported in this Table refer to those released in the final catalog. These numbers may differ from those reported in P09 since some redshifts have undergone revisions and corrections (see Sect. 3.1 and Appendix A).

considered. Serendipitous sources, which account for 21% of the sample, are usually faint neighbor of the primary targets and lie often at the edge of the 2D spectrum. Moreover, they are not color-selected as the primary LR-Blue targets, therefore, they may often lie at redshifts that are not accessible to the wavelength range covered by the chosen grism. The success rate for these objects is indeed relatively low (∼ 22%).

Figure 8 shows the z_{850} magnitudes as a funtion of redshift together with the histograms of redshift and z_{850} magnitude distribution. These plots show that objects with lower quality redshifts (C) tend to be very faint ($z_{850} > 24$) and have estimated redshifts in the range $1.8 < z < 2.2$. As already discussed in P09, objects with lower quality redshifts tend to have very faint magnitudes and have in general lower S/N spectra. Moreover, the higher failure rate observed for *BzK* galaxies and galaxies at $1.8 < z < 2.2$ may be explained by the fact that the Ly-α is often outside the spectral range covered by the LR-Blue grism (i.e. $\lambda < 3600$ Å) and by the fact that the VIMOS efficiency drops very quickly below 4000 Å (see also P09).

4.3. Success rate for VIMOS MR targets

We measured redshifts for 73% (69% including also the secondary serendipitous objects) of the observed MR spectra. In the VIMOS MR spectral campaign the overall success rate (i.e. redshift with quality A or B) is 58% and reaches 63% if only primary targets are considered.

Figure 9 shows the z_{850} magnitudes as a funtion of redshift for different redshift quality together with a histogram of the redshift distribution and a histogram of the distribution of z_{850} magnitudes for different redshift quality. Here we notice that the C flags are more frequent at $z > 0.8$, most probably due to the fact that above this redshift the main spectral features enter a wavelength range where both the OH sky emission lines and the CCD fringing are strong (i.e. at $\lambda > 7500$ Å), making line identification more difficult. We may also notice a slight trend with magnitude. As expected, lower quality flags peak at fainter magnitudes, due to the lower S/N of their spectra.

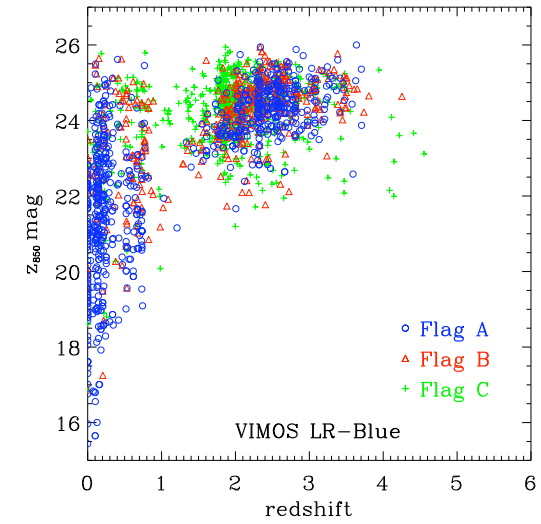

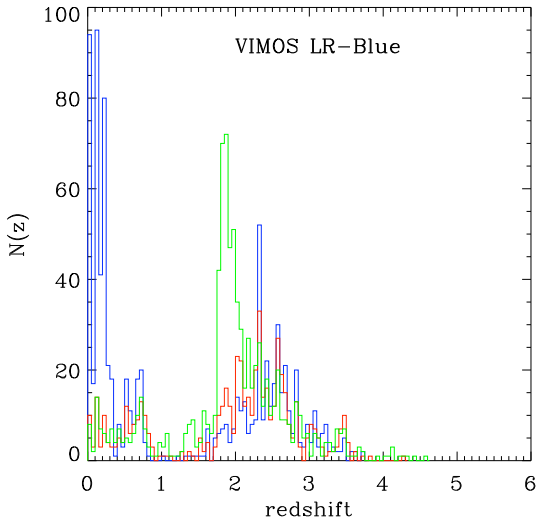

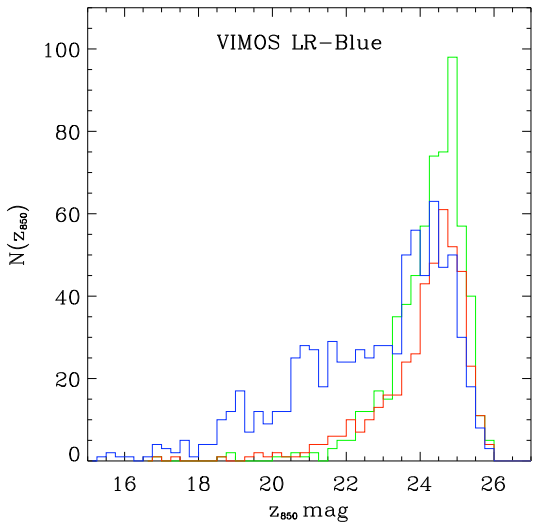

Fig. 8. VIMOS LR-Blue survey: GEMS z_{850} magnitudes versus redshift (*upper panel*), histogram of the redshift distribution (*middle panel*), and histogram of the z_{850} magnitude distribution (*lower panel*).

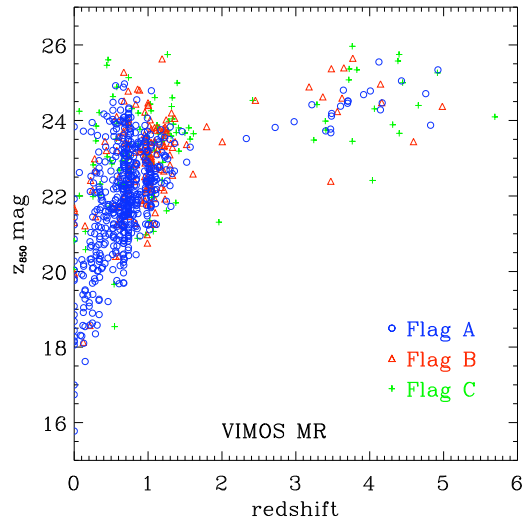

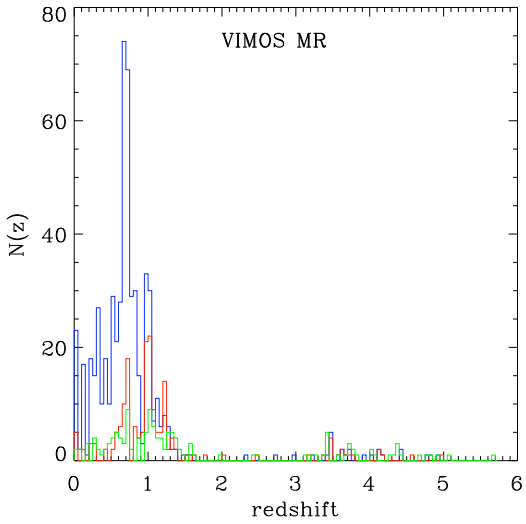

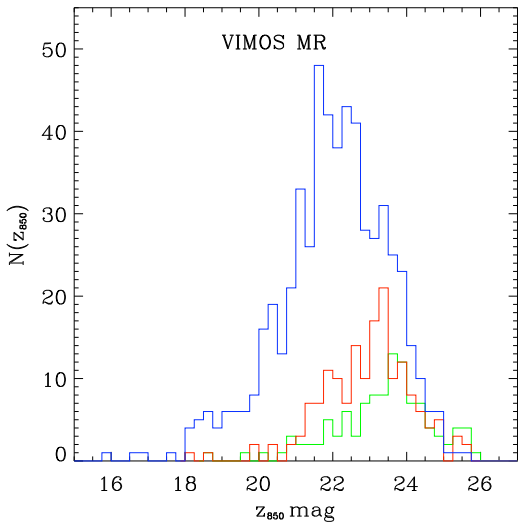

Fig. 9. VIMOS MR survey: GEMS z_{850} magnitudes versus redshift (*upper panel*), histogram of the redshift distribution (*middle panel*), and histogram of the z_{850} magnitude distribution (*lower panel*).

Table 3. Statistics of the GOODS/VIMOS MR campaign.

	MR				
P09[*] (6 masks)	**A**	**B**	**C**	**X**	**Total**
Num. of entries	458	112	85	295	950
Primary targets	433	98	70	215	816
Secondary targets	25	14	15	80	134
This work (4 masks)					
Num. of entries	170	88	63	147	468
Primary targets	148	75	43	115	381
Secondary targets	22	13	20	32	87
Total (10 masks)					
Num. of entries	628	200	148	442	1418
Primary targets	581	173	113	330	1197
Secondary targets	47	27	35	112	221

[*] For the first release (P09) the numbers of redshifts reported in this Table refer to those released in the final catalog. These numbers may differ from those reported in P09 since some redshifts have undergone revisions and corrections (see Sect. 3.1 and Appendix A).

4.4. Data products and redshift catalogs

The data products of the GOODS/VIMOS spectroscopic campaign released to the community[2] include, for each spectrum, the 1-dimensional spectrum in FITS format and the corresponding plot in postscript format.

We created two separated redshift catalogs: one for the VIMOS LR-Blue and one for the VIMOS MR campaign. In the two catalogs (see Table 4) we provide for each object: (column 1) the coordinate-based GOODS identification number, where the coordinates used are those of the matching WFI object, (column 2) the VIMOS identification number, (columns 3-4) the coordinates of the matching WFI object, (columns 5-6) the original VIMOS coordinates, (columns 7-10) B and R band WFI magnitudes with the corresponding errors, (columns 11-12) z_{850} GEMS magnitudes and corresponding errors, (column 13) redshift, (column 14) quality flag, (column 15) comments and identified spectral features, (column 16) a label for primary or secondary (i.e. serendipitous) objects, and (column 17) a label to distiguish between the first (P09) and second VIMOS release (this work).

For each grism we released two catalogs: one cleaned for duplicate observations of the same object, in which case we kept the best redshift estimate (with the only exception of objects having two quality-C redshifts, in which case we kept both estimates), and another containing the complete set of observations including duplicates. The final VIMOS LR-Blue catalog contains 3634 entries for 3271 individual targets and the final VIMOS MR catalog contains 1418 entries for 1294 individual targets.

5. Discussion

5.1. Redshift distribution and large scale structure

The fine-grain redshift distribution of galaxies in the VIMOS LR-Blue and MR catalogs is shown in Figure 7, where only objects with redshift quality A and B are plotted. We also plot the redshift distribution of the reference master catalog, described in Sect. 4.1, which collects 4227 objects (including stars) having high-quality redshift determinations (confidence level $\gtrsim$ 60%) from all the publicly available spectroscopic surveys in the CDFS. In order to standardize as much as possible the quality flag used in different surveys, we subdivided the master catalog into two subsamples: one including only "secure" redshifts (reliable at $\gtrsim$ 99% c.l.) comparable to VIMOS quality-A redshifts and another one including "likely" redshift determinations (reliable at $\sim$ 70 − 90% c.l.) comparable to VIMOS quality-B redshifts. A similar sample was used by P09 to assess the significance of the observed large scale structures. In P09 the significance of the observed peaks of the redshift distribution was investigated through a procedure similar to that used by Cohen et al. (1999) and Gilli et al. (2003): sources are distributed as a function of $V = c\ln(1+z)$, rather than z, where dV corresponds to the local velocity variation relative to the Hubble expansion. Simulations were used to assess the significance of the peaks in the redshift distribution. The procedure used in P09 allowed to confirm the presence of 14 peaks.

Here, we use the results of the previous analysis to investigate the spatial distribution of galaxies belonging to each of the 14 confirmed peaks, plus three additional tentative structures at $z \simeq 2.8$, $z \simeq 3.5$, and $z \simeq 3.7$ in our new, extended, reference master sample (see Fig. 10; see also Table B.1 and Fig. B.1–B.3 in the Appendix).

Three structures, having the size of small clusters/groups of galaxies, (i.e. at $z \simeq 0.53$, $z \simeq 0.67$, and $z \simeq 0.73$.) have associated extended X-ray emission. All of them are well-known structures, also observed by other spectroscopic surveys (e.g. GOODS-FORS2, K20).

The galaxies belonging to the cluster-like structure at $z \simeq 0.67$ are rather uniformly distributed on the whole CDFS area. Unfortunately, the extended X-ray source XID 645, most likely corresponding to the cluster core, lies in a region not entirely covered by the available spectroscopic surveys.

The second cluster-like structure, at $z \simeq 0.73$, is mostly composed of early-type galaxies concentrated around the central cD galaxy. The two extended X-ray sources (XID 566, 594) associated with this structure are located approximately at the position of the central cD galaxy and $\sim 5'$ to the north.

Another interesting cluster-like structure is the one at $z \sim 1.22$. The spatial distribution of the galaxies belonging to this structure is quite concentrated and elongated approximately along the east-west direction. Most of the galaxies in this sturcture are concentrated on an area of approximately $5'$ radius, corresponding to ~ 2.5 Mpc at $z = 1.22$.

It is worth noticing that several structures, including those at $z \simeq 2.3$ and $z \simeq 2.6$, extend over the entire surveyed area. This indicates that the size of these distant large structures must be of the order of $\sim 14 - 15$ Mpc.

At $z > 3$ no over-densities were confirmed by the previous analysis in P09. However, Kang & Im (2009) detected an overdensity of galaxies at $z \simeq 3.7$ using photometric redshifts. In Figure B.2 we plot the spatial distribution of galaxies belonging to the two furthest density peaks in the GOODS/CDFS, at $z \sim 3.48$ and $z \sim 3.70$, also observed by Vanzella et al. (2009). Interestingly, the 29 galaxies at $z \sim 3.48$ and the 11 galaxies at $z \sim 3.70$ appear to be concentrated around the same area.

5.2. Photometric selection of LBGs at $z \simeq 3$

Several photometric techniques have been used to select galaxies at $1 < z < 3$ in the various GOODS-S spectroscopic surveys. In P09 the reliability of the BzK and "sub"-U-dropouts selection criteria have been checked against contamination due to foreground interlopers.

[2] `http://archive.eso.org/cms/eso-data/data-packages`

Table 4. Spectroscopic redshift catalog for the GOODS/VIMOS LR-Blue campaign†. Columns list the following information: (1) coordinate-based GOODS identification number, (2) VIMOS identification number, (3-4) coordinates in WFI reference astrometry, (5-6) original VIMOS coordinates, (7-10) *B* and *R* band WFI magnitudes with the corresponding errors, (11-12) z_{850} GEMS magnitudes and corresponding errors, (13) redshift, (14) quality flag, (15) comments and identified spectral features, (16) label for primary or secondary (i.e. serendipitous) objects, and (17) label to distiguish between the first and second VIMOS release.

ID GOODS	ID VIMOS	RA_{WFI}	DEC_{WFI}	RA_{VIMOS}	DEC_{VIMOS}	*B* mag
(1)	(2)	(3)	(4)	(5)	(6)	(7)
J033133.01-274243.9	GOODS_LRb_002_1_q2_4_1	52.8875408	-27.7121947	52.8875408	-27.7121947	23.034
J033133.08-274301.0	GOODS_LRb_003_new_1_q2_3_1	52.8878231	-27.7169564	52.8878330	-27.7169530	25.590
J033133.44-274350.7	GOODS_LRb_001_1_q2_3_1	52.8893390	-27.7307466	52.8893390	-27.7307470	19.698
J033133.54-274303.6	GOODS_LRb_001_1_q2_6_1	52.8897394	-27.7176759	52.8897400	-27.7176700	21.711
J033133.91-274349.5	GOODS_LRb_001_1_q2_3_2	52.8913004	-27.7304179	52.8912850	-27.7304150	22.733
J033135.07-274256.4	GOODS_LRb_002_1_q2_8_1	52.8961455	-27.7156782	52.8961455	-27.7156782	21.322
J033135.85-274312.2	GOODS_LRb_003_new_1_q2_7_1	52.8993653	-27.7200705	52.8993610	-27.7200740	21.715
J033136.03-274328.9	GOODS_LRb_001_1_q2_11_1	52.9001304	-27.7246852	52.9001310	-27.7246880	20.268
J033136.08-274408.7	GOODS_LRb_002_1_q2_5_1	52.9003479	-27.7357574	52.9003479	-27.7357574	24.448
J033136.09-274240.3	GOODS_LRb_003_new_1_q2_10_1	52.9003640	-27.7111941	52.9003600	-27.7112160	24.406
J033136.18-274217.5	GOODS_LRb_001_1_q2_16_1	52.9007486	-27.7048485	52.9008030	-27.7048170	20.468
J033136.44-274421.9	GOODS_LRb_001_1_q2_8_1	52.9018278	-27.7394201	52.9018100	-27.7394120	25.134
J033136.53-274415.4	GOODS_LRb_003_new_1_q2_4_1	52.9022064	-27.7376119	52.9022140	-27.7376100	22.879
J033137.26-274220.6	GOODS_LRb_003_new_1_q2_13_1	52.9052472	-27.7057199	52.9052810	-27.7057650	24.442
J033137.27-274553.8	GOODS_LRb_002_1_q2_2_2	52.9053051	-27.7649414	52.9053051	-27.7649414	24.747

† Only a portion of the table is shown here for guidance regarding the form and content of the catalog. The entire table is available in electronic form at `http://archive.eso.org/cms/eso-data/data-packages`. The full table contains 17 columns of information on 3634 spectra.

Recently, deep VIMOS *U*-band photometry have been used to test another efficient criterion for the selection of Lyman Break Galaxies (Nonino et al. 2009). Here we use the $(U-B)$ and $(B-R)$ colors computed by Nonino et al. (2009) to test the reliability of the $(U-B)-(B-R)$ selection criterion on our VIMOS LR-Blue catalog of spectroscopic redshifts. Figure 11 shows the $(U-B)-(B-R)$ color–color diagram for VIMOS LR-Blue objects matching within an angular tolerance of $1''$ with *R*-band sources within the ACS image, having $23.5 \leq R_{MAG\_AUTO} \leq 27.0$, and error $\sigma(R_{MAG\_AUTO}) \leq 0.1$. Error bars in the plots are as in Nonino et al. (2009). The selection box is analogous to that defined in Nonino et al. (2009) with the only difference that here the WFI *B*-band filter is used instead of the ACS *B* filter. The plot of quality-A redshift estimates confirms that the selection box is quite efficient in selecting galaxies at $z > 2.8$. However, a small contamination by objects at smaller z is still present at $(U-B) < 1$. VIMOS LR-Blue quality-B redshifts are less reliable and show more mixing which may be due to mismatches in spectroscopic redshift measurements.

5.3. Ly-α EW vs UV Luminosity

After the completion of the GOODS/VIMOS spectroscopic campaign we identified a large number of LBGs: 288 in the LR-Blue campaign have a secure (i.e. quality flag=A) redshift at $2 \lesssim z \lesssim 4$ and 22 in the MR campaign have a secure at redshift $z \gtrsim 3$. Stacked spectra of all the LBGs available in the first release of the GOODS/VIMOS spectroscopic campaign were presented in P09.

Here, we extend and refine the previous analysis by collecting 288 LBGs with high-quality spectra in the LR-Blue campaign. In Fig. 12 we plot the composite spectra of two subsamples: 151 LBGs exhibiting Ly-α in emission (upper panel) and 137 with Ly-α in absorption (lower panel). Low-ionization interstellar absorption lines appear more pronounced in the composite spectrum of LBGs with Ly-α in absorption against a stronger UV continuum. The continuum has also a redder spectral slope for this population compared to the Ly-α emitters, consistent with other studies of $z \simeq 3$ LBGs samples (e.g. Shapley et al. 2003; Pentericci et al. 2007). This becomes more evident when the spectra of Ly-α "emitters" are stacked as a function of the Ly-α equivalent width (EW), as described below.

For the sub-sample of 151 Ly-α emitters we calculated the EW of the Ly-α and the absolute magnitude at 1450 Å (M_{145}). The EW was measured from the spectra by estimating the average continuum level from a spectral band immediatly red-ward of the Ly-α. Errors on the EWs were calculated by propagation of uncertainties, using the 1σ-error on the continuum. The absolute M_{145} magnitude was derived from the z_{850}-band, assuming a template of a star forming galaxy from Bruzual & Charlot (2003), with constant star formation and spectral slope $\beta \simeq -2$. Fig. 13 shows a comparison between the composite spectra of Ly-α emitters stacked in 4 bins of EW: 55 galaxies with EW< 10 Å, 62 with 10 Å <EW< 30 Å, 17 with 30 Å <EW< 50 Å, and 15 with EW> 50 Å. A trend of stronger absorption lines and redder spectral slopes with decreasing EW of the Ly-α is clearly evident. For a comparison, we also plot the stacked spectrum of LBGs with Ly-α in absorption, which extends the observed trends toward lower EWs.

In the redshift range probed by our sample ($2 \lesssim z \lesssim 4$), we find no clear evidence for a correlation between the EW of the Ly-α and redshift. In Fig. 14 we plot the distribution of EWs versus the absolute magnitude at 1450 Å. The plot shows the absence of large EW of Ly-α in bright galaxies, which confirms results based on different samples of Ly-α emitters and LBGs at $3 \lesssim z \lesssim 6$ (e.g. Shapley et al. 2003; Ajiki et al. 2003; Ando et al. 2006, 2007; Tapken et al. 2007; Verhamme et al. 2008; Vanzella et al. 2009; Pentericci et al. 2009).

The EW of the Ly-α line depends on the expansion velocity of the inter-stellar medium, the column density of neutral gas, the dust extinction, and the geometry (or the "clumpiness") of the medium. A possible explanation for the absence of strong Ly-α emission lines in the more luminous galaxies might be the presence of a more dusty and metal rich medium, residual of a recent, or still ongoing, burst of star formation and supernovae explosions in these galaxies.

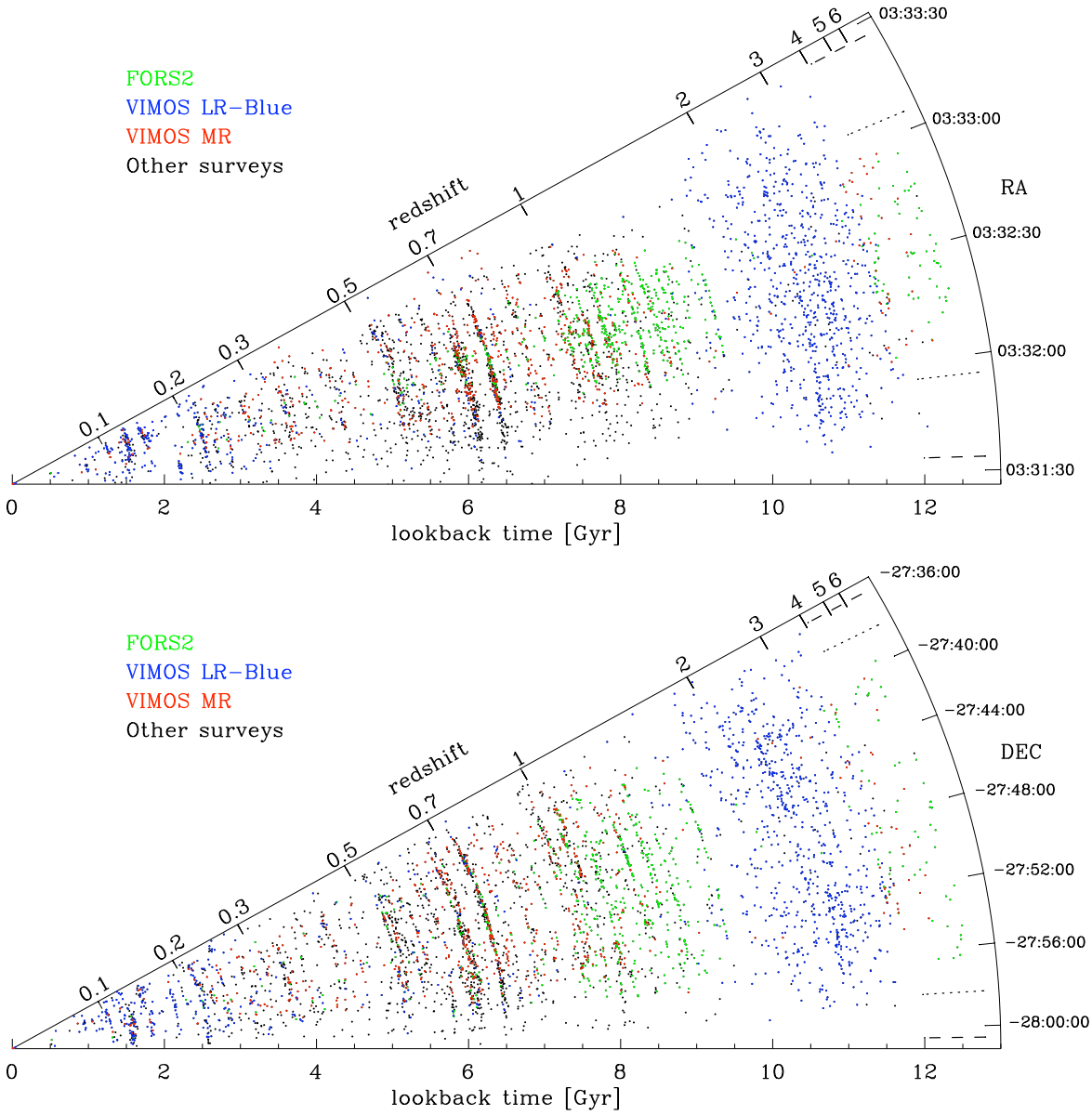

Fig. 10. Cone plots showing two projections of the spatial distribution of galaxies from the master catalog of redshifts of all the publicly available surveys in the CDFS described in the text (see Sect. 5.1 and Fig. 7). Different spectroscopic surveys are color-coded. The *dashed* and *dotted lines* indicate the approximate size of the 2Ms CDFS and the GOODS area, respectively. The angle of the cones has been arbitrarily stretched to help visualization.

5.4. New redshifts of X-ray sources

X-ray sources of the CDFS (Giacconi et al. 2002; Luo et al. 2008) and the ECDFS (Lehmer et al. 2005) have been targeted for follow-up optical spectroscopy (Szokoly et al. 2004, Silverman et al., in preparation). In this Section we present new (i.e. not yet published) redshifts for X-ray sources in the CDFS and ECDFS. We cross-correlated our VIMOS catalogs with both the 2Ms CDFS catalog of X-ray sources (Luo et al. 2008) and the catalog of the ECDFS (Lehmer et al. 2005). For the 2Ms CDFS catalog, we found 62 X-ray sources matching within an angular tolerance of 1″ objects having redshift determination in the VIMOS LR-Blue catalog and 42 in the VIMOS MR catalog. For the ECDFS catalog, we found 57 X-ray sources matching within a positional tolerance of 1″ objects having redshift determination in the VIMOS LR-Blue catalog and 17 in the VIMOS MR catalog.

In total 114 X-ray sources have been observed in the GOODS/VIMOS spectroscopic campaign. In Table 5 we list 12 new (not yet published) redshifts, either unknown before or improving previous estimates, obtained from the last 8 VIMOS masks released in this paper. Spectra and finding charts of these sources can be found in the Appendix C.

6. Conclusions

After the completion of the two complementary ESO/GOODS spectroscopic campaigns carried out with FORS2 (Vanzella et al. 2005, 2006, 2008) and VIMOS (P09 and this work), a very large sample of galaxies in the CDFS has been spectroscopically targeted. In this paper we presented the final data release, including also data from the previous release (P09), of the GOODS/VIMOS spectroscopic campaign, which was organized

Table 5. List of 12 new spectroscopic redshifts for X-ray sources of the 2Ms CDFS catalog (Luo et al. 2008) and of the ECDFS catalog (Lehmer et al. 2005). Columns list the following information: (1) coordinate-based GOODS identification number, (2) VIMOS identification number, (3-4) coordinates in WFI reference astrometry, (5) X-ray identification number from (Luo et al. 2008), (6) X-ray identification number from (Lehmer et al. 2005), (7) redshift, (8) quality flag, and (9) comments and identified spectral features.

GOODS_ID	VIMOS_ID	RA	DEC	XID		z	Q	Comments
(1)	(2)	(3)	(4)	(5)	(6)	(7)	(8)	(9)
J033143.17-274131.0	GOODS_LRb_002_1_q2_33_1	52.929871	-27.691935	-	135	2.9981	C	Lyα(em),CIV(em)
J033146.45-274123.6	GOODS_LRb_002_1_q2_44_1	52.943559	-27.689879	-	160	0.6646	B	OII
J033155.33-274313.6	GOODS_LRb_002_1_q2_61_1	52.980564	-27.720448	-	225	0.8610[a]	B	MgII,FeII
J033214.98-274225.0	GOODS_LRb_002_1_q1_6_1	53.062400	-27.706952	145	340	2.6087*	B	Lyα(abs),OI,CII,AlIII
J033216.13-275644.0	GOODS_LRb_002_1_q3_65_1	53.067204	-27.945558	157	344	2.6667[b]	A	Lyα(em),SiIV,CIV (BLAGN)
J033218.25-275224.9	GOODS_MR_dec06_2_q2_19_1	53.076059	-27.873578	175	-	0.7396	A	OII,Hβ,OIII
J033220.05-274447.3	GOODS_LRb_002_1_q1_8_1	53.083537	-27.746460	188	357	1.8930*	B	CIV,CIII] (BLAGN)
J033225.69-273941.2	GOODS_LRb_dec06_3_q1_2_1	53.107044	-27.661458	-	370	0.0010	A	Star
J033244.61-274835.9	GOODS_LRb_002_1_q4_66_1	53.185862	-27.809984	372	-	2.5860*	A	Lyα(em),OI,CIV,FeII
J033250.25-275251.9	GOODS_MR_dec06_3_q3_2_2	53.209362	-27.881094	402	480	3.4742	B	Lyα(em)
J033304.81-274731.7	GOODS_LRb_dec06_1_q4_69_1	53.270059	-27.792149	445	-	2.0265	A	Lyα(em),CIV,HeII,CIII] (BLAC
J033306.80-274626.6	GOODS_LRb_dec06_1_q4_79_2	53.278332	-27.774065	-	571	1.7048	A	SiIV,SiII,CIV,FeII,AlII

* Redshift more reliable compared to previously published estimates.
[a] Redshift more reliable then the second available measurement: GOODS_LRb_dec06_1_q2_15_2 z = 2.3634 flag C.
[b] Redshift resulting from average of two measurements: GOODS_LRb_002_1_q3_65_1 z = 2.6652 flag A and GOODS_LRb_dec06_1_q3_16_1 z = 2.6681 flag A.

in two separated campaign: one using the LR-Blue grism and one using the MR grism.

The main outcome for the LR-Blue campaign can be summarized as follows:

– a total of 3634 spectra has been extracted, providing 2242 redshift measurements with a typical $\sigma_z \simeq 0.0012$ ($\sim 255\,\mathrm{km\,s^{-1}}$). We obtained a redshift determination for 2040 out of the 3271 individual targets observed. We assigned a quality flag to the redshift measurements, which provides an estimate of their reliability. The reliability of VIMOS LR-Blue redshifts with quality flag A, B, and C is estimated to be approximately 100%, 60%, and 20% confidence level, respectively. The number of redshifts determinations above the 60% c.l. (i.e. flag A+B) amounts to 1395.

For the MR campaign the main results can be summarized as follows:

– a total of 1418 spectra has been extracted, providing 976 redshift measurements with a typical $\sigma_z \simeq 0.00040$ ($\sim 120\,\mathrm{km\,s^{-1}}$). We obtained a redshift determination for 882 out of the 1294 individual targets observed. VIMOS MR quality flag-A, -B, and -C redshifts are estimated to be reliable at approximately 100%, 95%, and 60% confidence level, respectively.

We complemented our VIMOS spectroscopic catalog with all existing spectroscopic redshifts publicly available in the CDFS and obtained a redshift master catalog with 7332 entries. We used good-quality redshifts (c.l. > 60%) to investigate the spatial distribution of galaxies in 16 peaks of the redshift distribution, tracing large scale structures out to $z \simeq 3.7$.

Stacked spectra of LBGs were produced in a few bins of Ly-α EW. We found evidence for a lack of bright objects with high EW of the Ly-α, which confirms results based on different samples of Ly-α emitters and LBGs at $3 \lesssim z \lesssim 6$ (e.g. Shapley et al. 2003; Ajiki et al. 2003; Ando et al. 2006, 2007; Tapken et al. 2007; Verhamme et al. 2008; Vanzella et al. 2009; Pentericci et al. 2009).

Additionally, we obtained new redshifts for 12 X-ray sources of the CDFS and ECDFS. These sources also appear in the new catalog of X-ray sources detected in the ECDFS, which includes the identification of optical and near-IR counterparts (Silverman et al., in preparation).

The reduced spectra and the redshift catalogs are released to the community and can be retrieved in electronic form at *http://archive.eso.org/cms/eso-data/data-packages*. These data, in combination with the other spectroscopic campaigns in the GOODS-S field, represent an essential contribution to achieve the scientific goals of GOODS, providing the lookback time across which the evolution of galaxy masses, morphologies, clustering, and star formation can be traced.

Acknowledgements. We acknowledge the ESO staff in Paranal and Garching for the help in the development of this program (ESO program 171.A-3045 *The Great Observatories Origins Deep Survey: ESO Public Observations of the SIRTF Legacy/HST Treasury/Chandra Deep Field South*.).

References

Ajiki, M., Taniguchi, Y., Fujita, S. S., et al. 2003, AJ, 126, 2091
Ando, M., Ohta, K., Iwata, I., et al. 2006, ApJ, 645, L9
Ando, M., Ohta, K., Iwata, I., et al. 2007, PASJ, 59, 717
Bruzual, G. & Charlot, S. 2003, MNRAS, 344, 1000
Bunker, A. J., Stanway, E. R., Ellis, R. S., McMahon, R. G., & McCarthy, P. J. 2003, MNRAS, 342, L47
Cimatti, A., Mignoli, M., Daddi, E., et al. 2002, A&A, 392, 395
Cohen, J. G., Blandford, R., Hogg, D. W., Pahre, M. A., & Shopbell, P. L. 1999, ApJ, 512, 30
Cristiani, S., Appenzeller, I., Arnouts, S., et al. 2000, A&A, 359, 489
Croom, S. M., Warren, S. J., & Glazebrook, K. 2001, MNRAS, 328, 150
Daddi, E., Cimatti, A., Renzini, A., et al. 2004, ApJ, 617, 746
Dickinson, M., Giavalisco, M., & The Goods Team. 2003, in The Mass of Galaxies at Low and High Redshift, ed. R. Bender & A. Renzini, 324–+
Dickinson, M., Stern, D., Giavalisco, M., et al. 2004, ApJ, 600, L99
Giacconi, R., Zirm, A., Wang, J., et al. 2002, ApJS, 139, 369
Giavalisco, M., Ferguson, H. C., Koekemoer, A. M., et al. 2004, ApJ, 600, L93
Gilli, R., Cimatti, A., Daddi, E., et al. 2003, ApJ, 592, 721
Grazian, A., Fontana, A., de Santis, C., et al. 2006, A&A, 449, 951
Kang, E. & Im, M. 2009, ApJ, 691, L33
Le Fèvre, O., Vettolani, G., Garilli, B., et al. 2005, A&A, 439, 845
LeFevre, O., Saisse, M., Mancini, D., et al. 2003, in Society of Photo-Optical Instrumentation Engineers (SPIE) Conference Series, Vol. 4841, Society

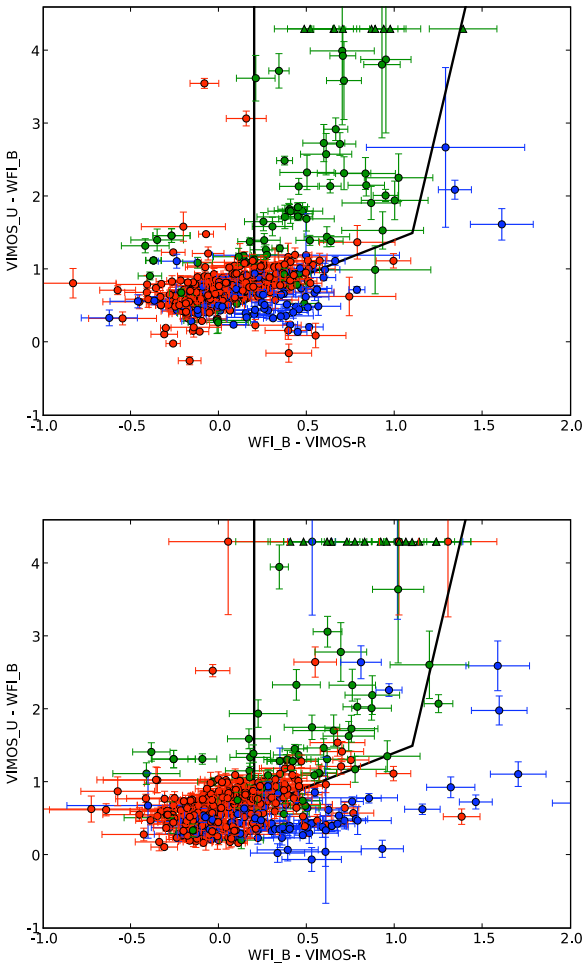

Fig. 11. $(U-B)-(B-R)$ color–color diagrams for VIMOS LR-Blue objects matching with R-band sources, $23.5 \leq R_{MAG\_AUTO} \leq 27.0$, and $\sigma(R_{MAG\_AUTO}) \leq 0.1$, and having redshift quality flag A *(upper panel)* and B *(lower panel)*. The redshift is color coded: objects at $z < 1.8$ in blue, $1.8 \leq z \leq 2.8$ in red, and $z > 2.8$ in green. Triangles denote lower limits at 1σ c.l. (30 AB magnitude in U band).

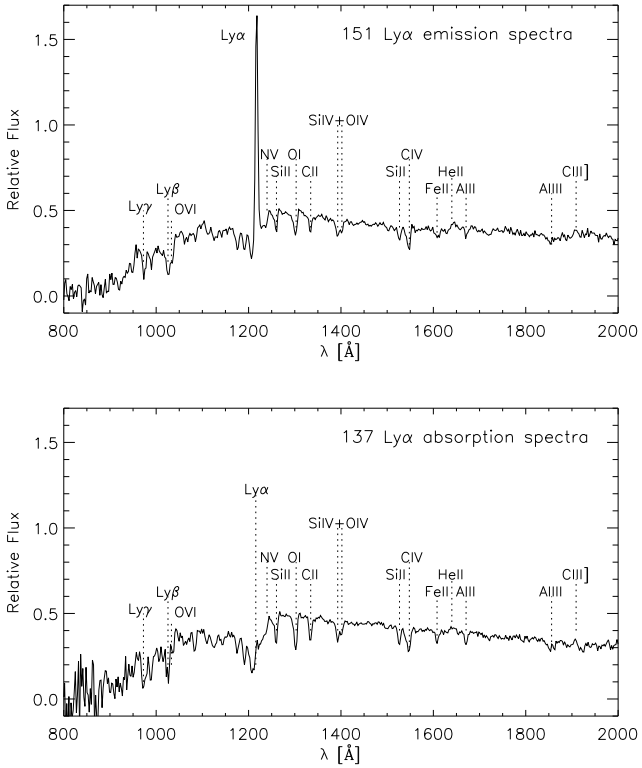

Fig. 12. Co-added LR-Blue spectra of 151 LBGs with Ly-α in emission *(upper panel)* and 137 with Ly-α in absorption *(lower panel)*. Only high-quality (i.e. quality flag=A) spectra of LBGs at $2 < z < 4$ have been selected for stacking.

of Photo-Optical Instrumentation Engineers (SPIE) Conference Series, ed. M. Iye & A. F. M. Moorwood, 1670–1681
Lehmer, B. D., Brandt, W. N., Alexander, D. M., et al. 2005, ApJS, 161, 21
Luo, B., Bauer, F. E., Brandt, W. N., et al. 2008, ApJS, 179, 19
Mignoli, M., Cimatti, A., Zamorani, G., et al. 2005, A&A, 437, 883
Nonino, M., Dickinson, M., Rosati, P., et al. 2009, Accepted for publication on ApJS
Pentericci, L., Grazian, A., Fontana, A., et al. 2009, A&A, 494, 553
Pentericci, L., Grazian, A., Fontana, A., et al. 2007, A&A, 471, 433
Popesso, P., Dickinson, M., Nonino, M., et al. 2009, A&A, 494, 443
Ravikumar, C. D., Puech, M., Flores, H., et al. 2007, A&A, 465, 1099
Renzini, A., Cesarsky, C., Cristiani, S., et al. 2003, in The Mass of Galaxies at Low and High Redshift, ed. R. Bender & A. Renzini, 332–+
Scodeggio, M., Franzetti, P., Garilli, B., et al. 2005, PASP, 117, 1284
Shapley, A. E., Steidel, C. C., Pettini, M., & Adelberger, K. L. 2003, ApJ, 588, 65
Stanway, E. R., Bunker, A. J., McMahon, R. G., et al. 2004, ApJ, 607, 704
Strolger, L.-G., Riess, A. G., Dahlen, T., et al. 2004, ApJ, 613, 200
Szokoly, G. P., Bergeron, J., Hasinger, G., et al. 2004, ApJS, 155, 271
Tapken, C., Appenzeller, I., Noll, S., et al. 2007, A&A, 467, 63
van der Wel, A., Franx, M., van Dokkum, P. G., & Rix, H.-W. 2004, ApJ, 601, L5
Vanzella, E., Cristiani, S., Dickinson, M., et al. 2008, A&A, 478, 83
Vanzella, E., Cristiani, S., Dickinson, M., et al. 2005, A&A, 434, 53
Vanzella, E., Cristiani, S., Dickinson, M., et al. 2006, A&A, 454, 423
Vanzella, E., Giavalisco, M., Dickinson, M., et al. 2009, ApJ, 695, 1163
Verhamme, A., Schaerer, D., Atek, H., & Tapken, C. 2008, A&A, 491, 89

Appendix A: Corrections to previous release

We revised some of the redshifts from the first release of the GOODS/VIMOS survey for objects that were observed more than once in the GOODS/VIMOS survey or in other surveys. After comparing their spectra, 7 redshift determinations were modified as follows:

- GOODS_LRb_001_1_q1_51_1 at $z = 2.2077$ (flag A) in the previous release, was observed also with FORS2 (GDS J033226.67-274013.4). The low-S/N UV absorption lines were misclassified in the VIMOS spectrum. Instead, thanks to the comparison with the FORS2 spectrum, CIII] in emission could be identified. The new redshift obtained, $z = 1.6045$, with quality flag B, is in agreement with the FORS2 measurement ($z = 1.612$, flag A).
- GOODS_LRb_003_new_q1_61_1 at $z = 0.067$ (flag A) in the previous release. A possibly broad CIII] emission line was previously identified as [OII]. This object was also observed by Silverman et al. (in preparation), where the measured redshift is $z = 1.089$. Our new estimate of the redshift based on CIII] and FeII lines is in agreement with the more recent measurement. We find $z = 1.0890$ with quality flag B.
- GOODS_LRb_003_new_q3_11_1 at $z = 2.6114$ (flag B) in the previous release. This object was also observed in another mask (GOODS_LRb_003_new_2_q3_30_1, $z = 2.5831$, flag B). Both estimates are based on the detection of a Ly-α

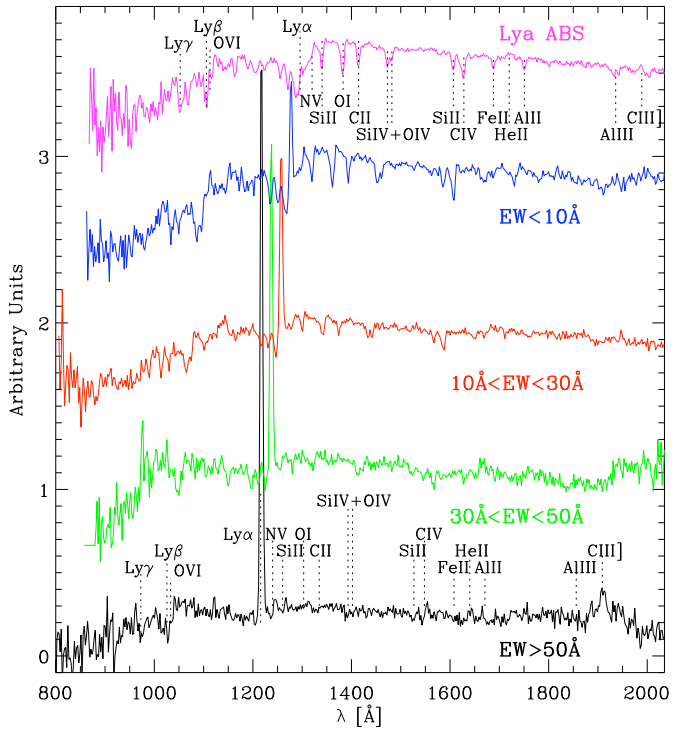

Fig. 13. Co-added LR-Blue spectra of LBGs with Ly-α in emission. Spectra are stacked as a function of rest frame EW of the Ly-α. We defined 4 bins of EW as follows: EW< 10 Å (55 galaxies), 10 Å <EW< 30 Å (62 galaxies), 30 Å <EW< 50 Å (17 galaxies), and EW> 50 Å (15 galaxies). We also plot the stacked spectrum of the 137 LBGs with Ly-α in emission for a comparison. The spectra have been offset by an arbitrary factor along both axes for easier viewing.

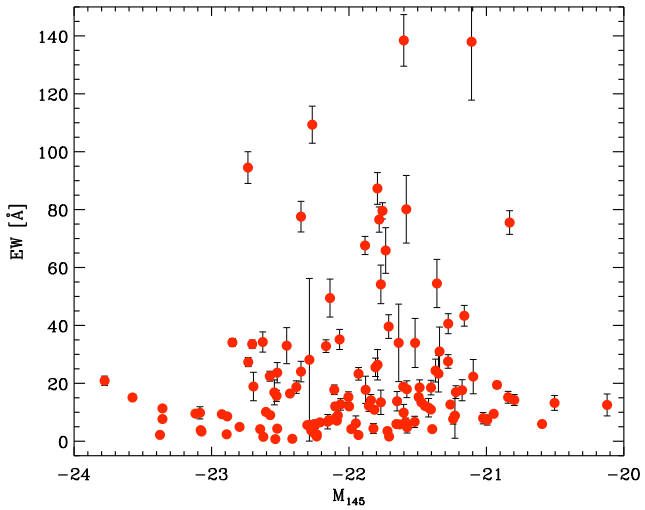

Fig. 14. Rest frame Ly-α EW as a function of UV luminosity (M_{145}, absolute magnitude at 1450 Å). Error bars refer to 1σ confidence level.

in emission. However, we noticed that the former measurement required a slight adjustment (i.e. the Ly-α was correctly identified, but slightly misaligned). The new resulting redshift, $z = 2.5882$, with quality flag B, is in better agreement with the second VIMOS measurement.

– GOODS_LRb_003_new_1_q3_68_1 at $z = 0.7297$, flag C based on the identification of [OII]. The redshift is correct and it is confermed by a second observation in a MR mask (GOODS_MR_new_1_d_q2_32_1 at $z = 0.7308$, flag A). We simply upgraded the quality flag from C to B in this case.
– GOODS_LRb_003_new_2_q1_42_1 at $z = 2.1084$ (flag B) in the previous release. The broad MgII emission line was misclassified as Ly-α. This object was also observed in one of the new reduced masks (GOODS_LRb_dec06_3_q1_46_2, $z = 0.7358$, flag A). Two spectral features are clearly identified: a broad emission line from MgII and [OII]. Therefore, the new redshift assigned is $z = 0.7357$ with quality flag A.
– GOODS_MR_new_1_d_q3_2_1 at $z = 0.5107$ (flag B) in the previous release. Two spectral features were misclassified: [OIII] and Hβ. Thanks to the comparison with a second observation of this object (GOODS_MR_001_q4_3_1 $z = 1.0338$, flag A), we identified [OII] and MgII instead. The new redshift estimate is $z = 1.0349$ with quality flag B.

The following redshifts were also revised:

– GOODS_LRb_001_1_q2_66_1 at $z = 0.240$ (flag B) in the previous release. The broad MgII emission line was misclassified as [OII]. After revising the spectrum we could identify some typical AGN features (e.g. a broad MgII emission line and broad Fe bump at ~2960 Å) plus [OII] and Ca H and K. The new redshift obtained is $z = 0.6632$ (flag A).
– GOODS_LRb_001_1_q3_5_3 at $z = 0.076$ (flag B) in the previous release. The spectrum shows only one visible emission line at $\sim$ 4000 Å, which was previously interpreted as [OII]. For this object we find more likely the identification as Ly-α in emission, which gives a new tentative redshift of $z = 2.2980$ (flag C).
– GOODS_LRb_001_q4_44_1 and GOODS_LRb_003_new_q4_28_1 at $z = 1.6285$ (flag B) in the previous release. We reviewed the redshifts of the two spectra for this object, which were based on the identification of two very broad emission lines (i.e. CIV and CIII]). In addition, we identified several absorption lines (e.g. FeII, AlIII) that helped further calibrating the redshifts. The new measurements are $z = 1.609$ (flag A) and $z = 1.608$ (flag A) for GOODS_LRb_001_q4_44_1 and GOODS_LRb_003_new_q4_28_1, respectively.
– GOODS_LRb_003_new_1_q2_46_2 is the same object as GOODS_LRb_001_1_q2_66_1 (see above). The new redshift measurement is $z = 0.6649$ (flag A).
– GOODS_LRb_003_new_1_q4_63_2 at $z = 0.585$ (flag C) in the previous release. The spectrum is red, but quite noisy and may resemble that of an elliptical galaxy. However, after the inspection of the WFI R-image and the ACS z-image of this object, we found that a more likely explanation might be given in terms of a star. Therefore, we assign $z = 0.000$ and flag B to this object.
– GOODS_MR_new_2_b_q4_15_1 at $z = 5.2936$ (flag C) in the previous release. We could identify Ca H and K, Fe I and possibly [OII]. The new redshift assigned to this object is $z = 0.9250$ with quality flag B.

Appendix B: Large scale structure

Table B.1 and Fig. B.1–B.3 show the results of the analysis of the spatial distribution of the 14 confirmed density peaks, plus three additional tentative structures at $z \simeq 2.8$, $z \simeq 3.5$, and $z \simeq 3.7$, observed in the master catalog of redshifts of the CDFS, described in Sect. 5.1.

Table B.1. List of observed peaks in the redshift distribution of the reference master catalog. The columns list: (1) the average $< z >$ of each peak, (2) the velocity dispersion σ_V, (3) the redshift range corresponding to $\pm 2\sigma_V$, selected for the analysis of the spatial distribution (see Fig. B.1, B.2, and B.3), (4) the number of galaxies in the selected redshift interval, and (5) the identification numbers of extended X-ray sources (from Giacconi et al. 2002) associated with the peak.

$< z >$	σ_V [km/s]	$z_{min} - z_{max}$	N	XID
(1)	(2)	(3)	(4)	(5)
0.126	906	0.119 – 0.133	73	–
0.215	443	0.211 – 0.218	61	–
0.338	1724	0.322 – 0.353	76	–
0.530	2190	0.508 – 0.552	193	–
0.672	1758	0.653 – 0.692	306	645
0.735	565	0.728 – 0.742	257	566, 594
0.973	2936	0.935 – 1.012	181	249
1.039	859	1.028 – 1.051	110	–
1.095	1536	1.074 – 1.117	129	–
1.221	391	1.215 – 1.227	65	–
1.296	261	1.292 – 1.300	35	–
1.611	497	1.602 – 1.620	36	–
2.318	2102	2.272 – 2.365	108	–
2.566	1435	2.532 – 2.601	72	–
2.811	575	2.796 – 2.825	23	–
3.471	984	3.442 – 3.501	29	–
3.702	360	3.691 – 3.714	11	–

Appendix C: Spectra of X-ray sources with new redshift determinations

In Fig. C.1, C.2, and C.3 we show 12 VIMOS spectra of X-ray sources with new redshift determinations (i.e. either unknown before or improving previous estimates), obtained from the last 8 VIMOS masks released in this paper. Together with each spectrum we provide a finding chart with the position of the corresponding X-ray sources. These sources also appear in the new catalog of X-ray sources detected in the ECDFS, which includes the identification of optical and near-IR counterparts (Silverman et al., in preparation).

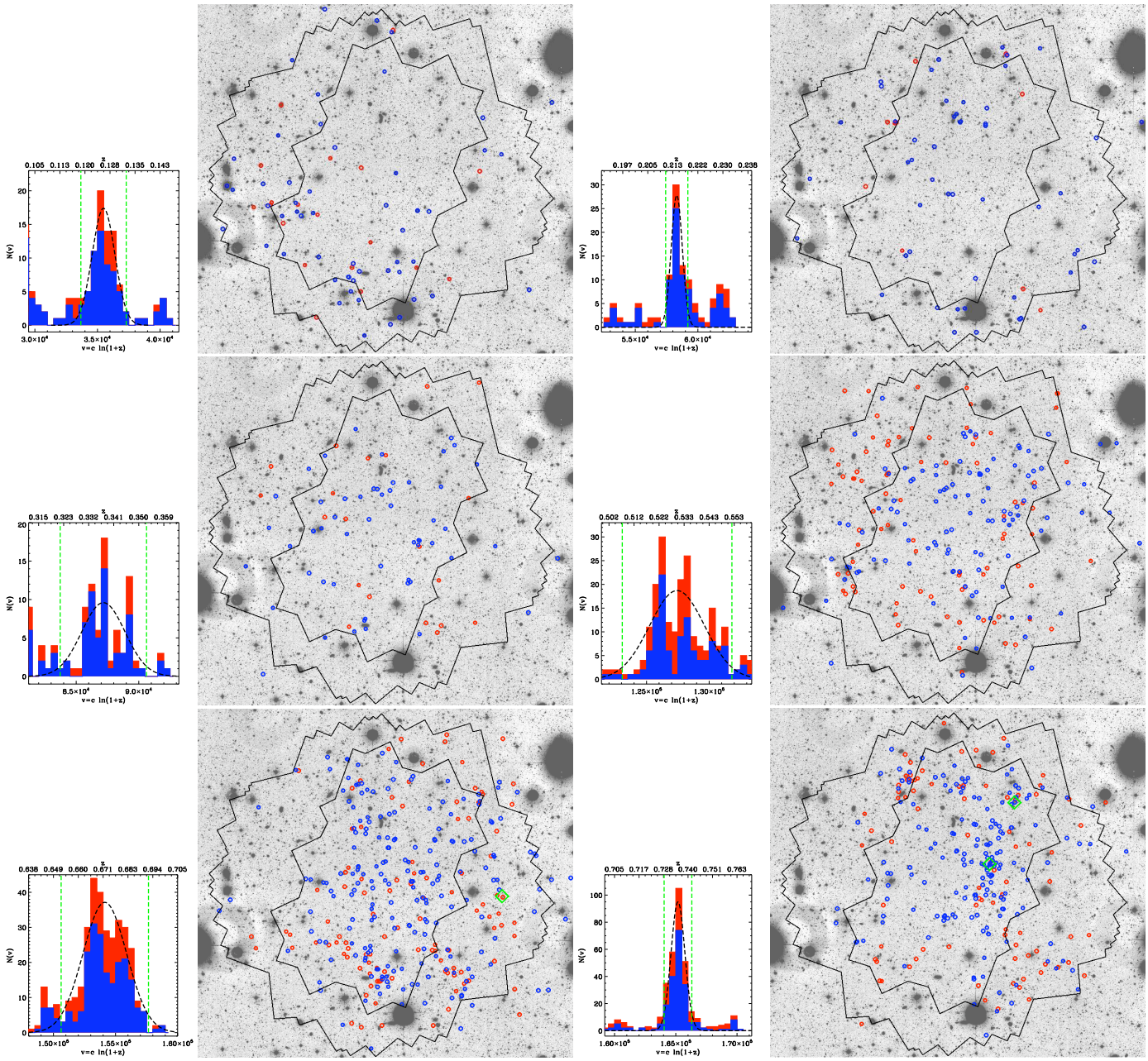

Fig. B.1. Histograms of the velocity distribution, $V = c\ln(1+z)$, and spatial distribution of galaxies belonging to each of the density peak listed in Table B.1. For each structure, we display "secure" redshifts (> 99% c.l.) in *blue* and "likely" redshifts (~ 70 – 90% c.l.) in *red*. The histograms show the Gaussian fit to the peak of the velocity distribution (*black dashed curve*) and the 2σ-intervals around the peak selected for the spatial analysis (*vertical green dashed lines*). All the histograms are binned to $\Delta V = 500$ km/s. The green diamonds show the position of the extended X-ray sources (i.e. XID 645 at $z \sim 0.67$; XID 566 and XID 594 at $z \sim 0.73$; XID 249 at $z \sim 0.97$). The black contours indicate the GOODS area and the field coverage of the 2Ms Chandra exposure.

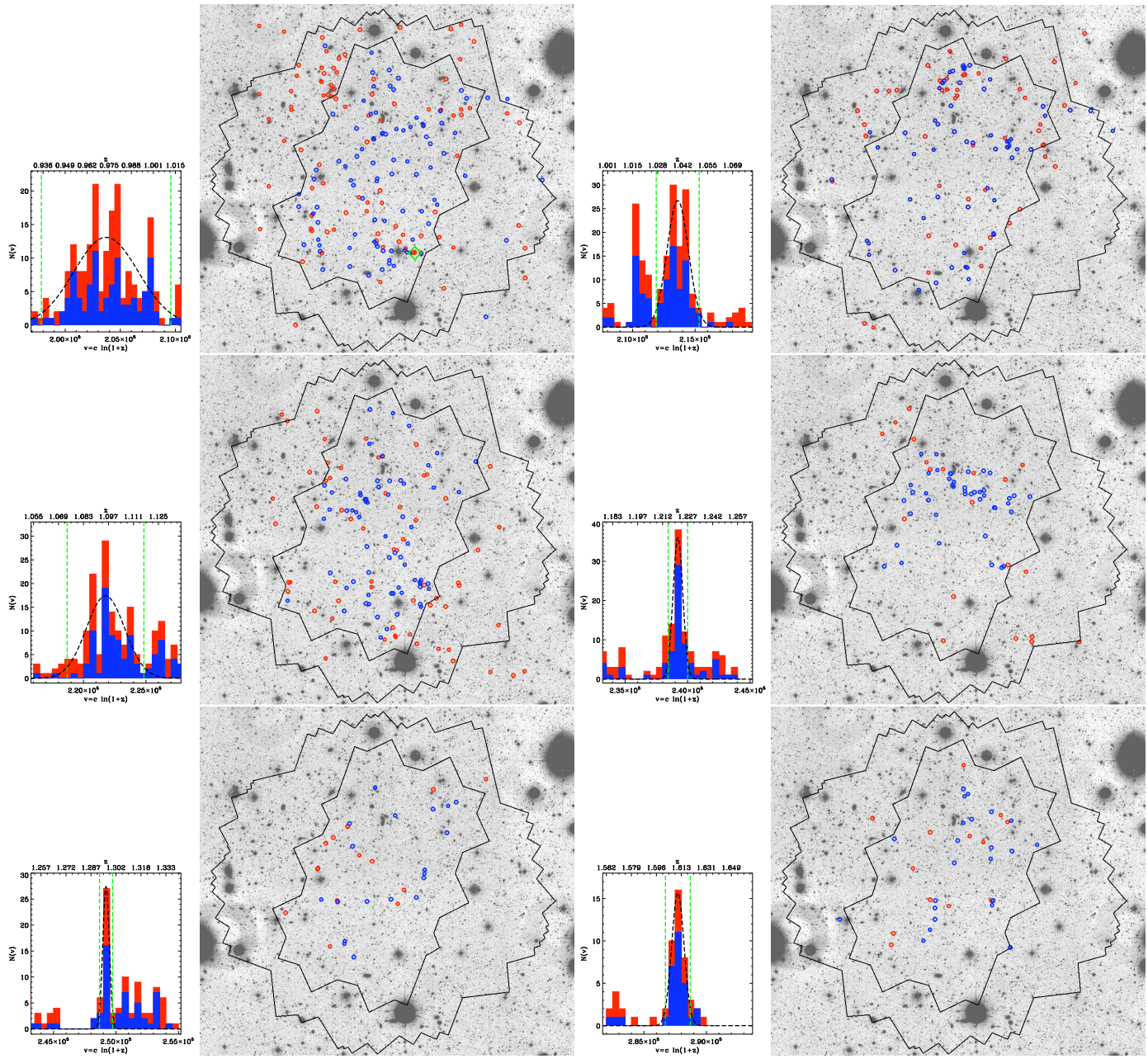

Fig. B.2. Histograms of the velocity distribution, $V = c\ln(1+z)$, and spatial distribution of galaxies belonging to each of the density peak listed in Table B.1. For each structure, we display "secure" redshifts (> 99% c.l.) in *blue* and "likely" redshifts (~ 70 – 90% c.l.) in *red*. The histograms show the Gaussian fit to the peak of the velocity distribution (*black dashed curve*) and the 2σ-intervals around the peak selected for the spatial analysis (*vertical green dashed lines*). All the histograms are binned to $\Delta V = 500$ km/s. The black contours indicate the GOODS area and the field coverage of the 2Ms Chandra exposure.

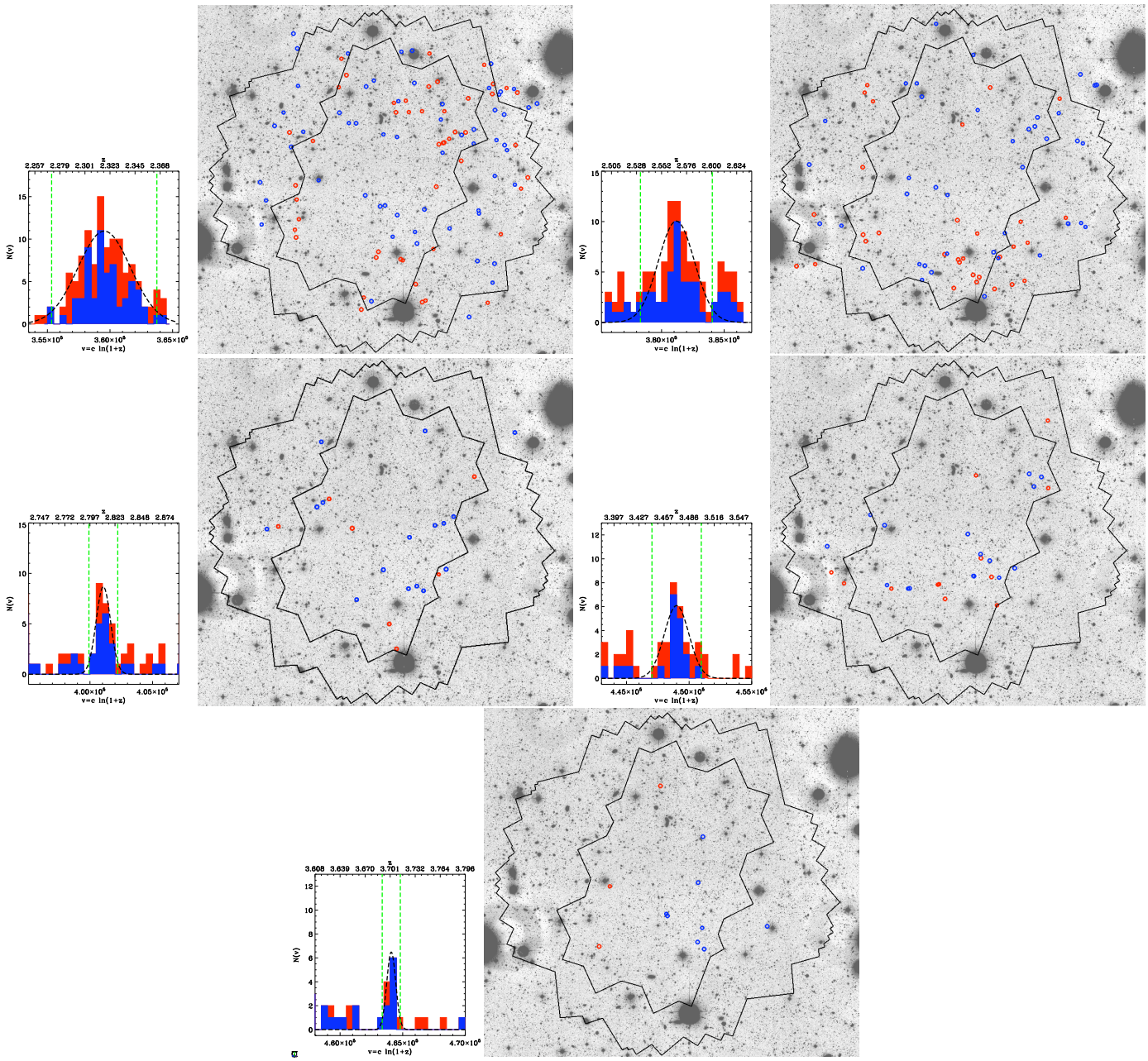

Fig. B.3. Histograms of the velocity distribution, $V = c\ln(1+z)$, and spatial distribution of galaxies belonging to each of the density peak listed in Table B.1. For each structure, we display "secure" redshifts (> 99% c.l.) in *blue* and "likely" redshifts (~ 70 – 90% c.l.) in *red*. The histograms show the Gaussian fit to the peak of the velocity distribution (*black dashed curve*) and the 2σ-intervals around the peak selected for the spatial analysis (*vertical green dashed lines*). All the histograms are binned to $\Delta V = 500$ km/s. The black contours indicate the GOODS area and the field coverage of the 2Ms Chandra exposure.

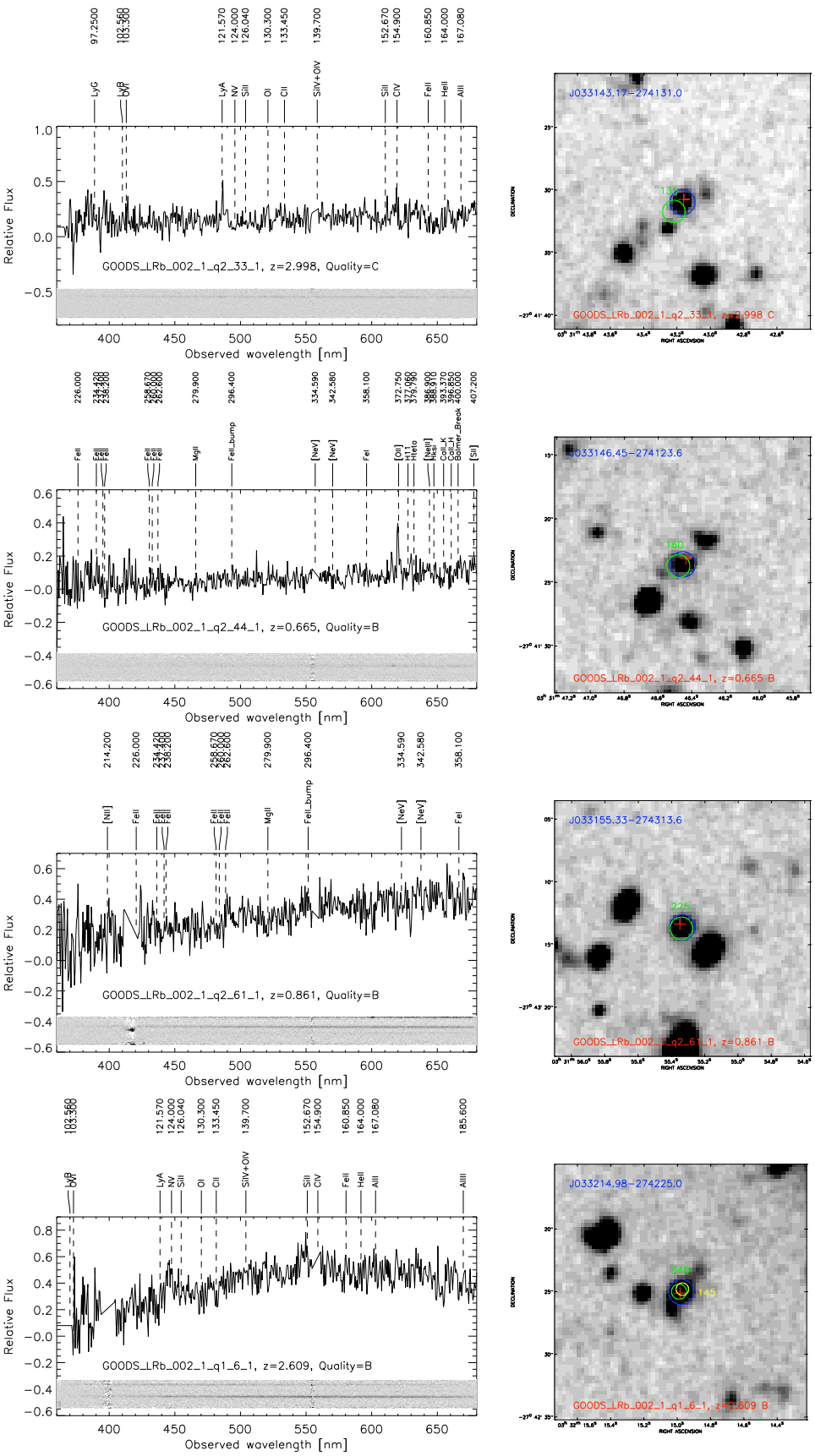

Fig. C.1. New VIMOS spectra of X-ray sources with WFI R-band 20″ × 20″ cutout centered on the position of the matching WFI source. Red crosses indicate the reconstructed VIMOS coordinates. The blue circles show the position of the WFI-matched objects. The yellow and green circles display the position of X-ray sources from the 2Ms CDFS or from the ECDFS catalog, respectively. Labels with corresponding colors indicate source identification numbers.

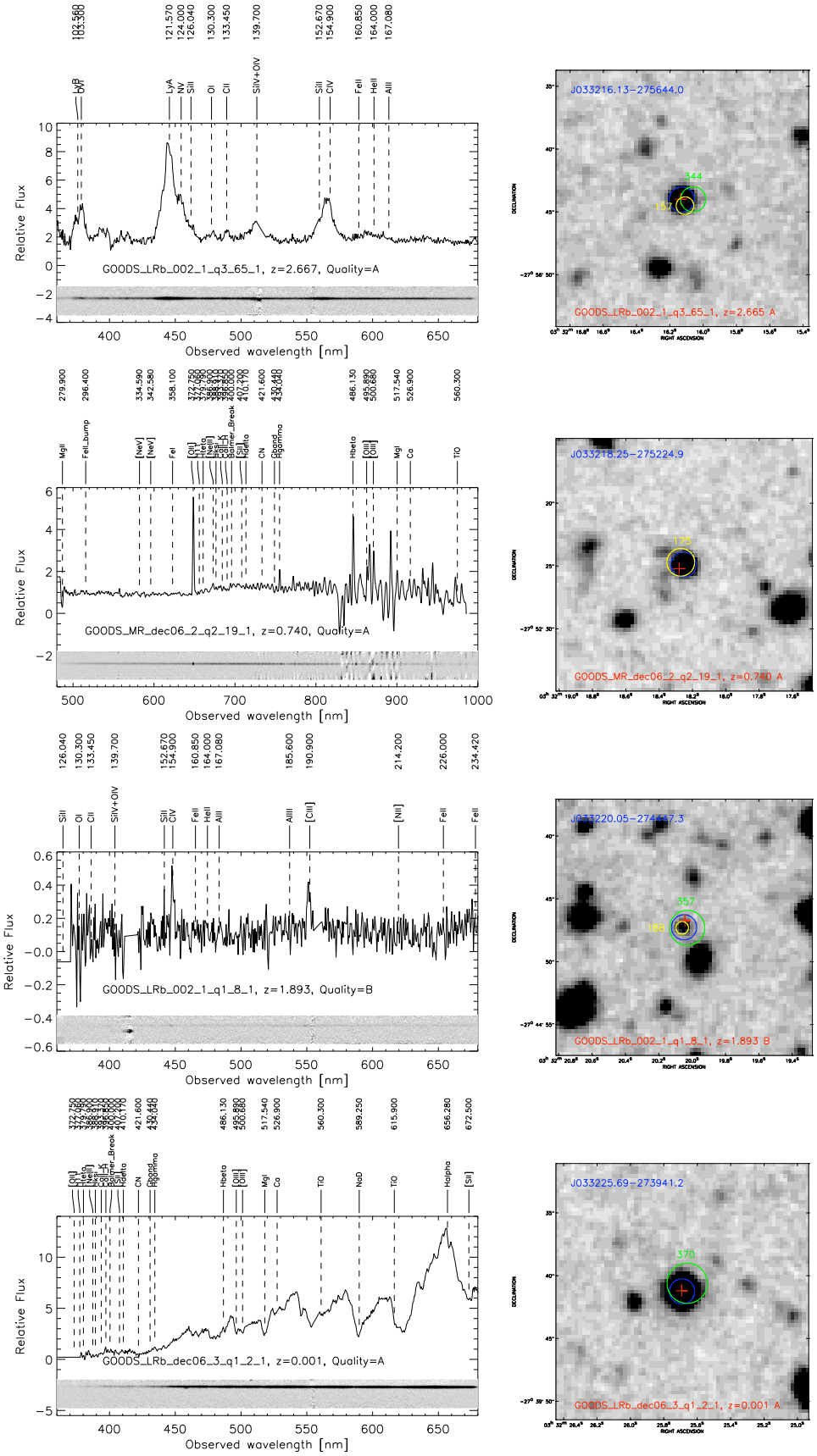

Fig. C.2. New VIMOS spectra of X-ray sources with WFI *R*-band 20″ × 20″ cutout centered on the position of the matching WFI source. Red crosses indicate the reconstructed VIMOS coordinates. The blue circles show the position of the WFI-matched objects. The yellow and green circles display the position of X-ray sources from the 2Ms CDFS or from the ECDFS catalog, respectively. Labels with corresponding colors indicate source identification numbers.

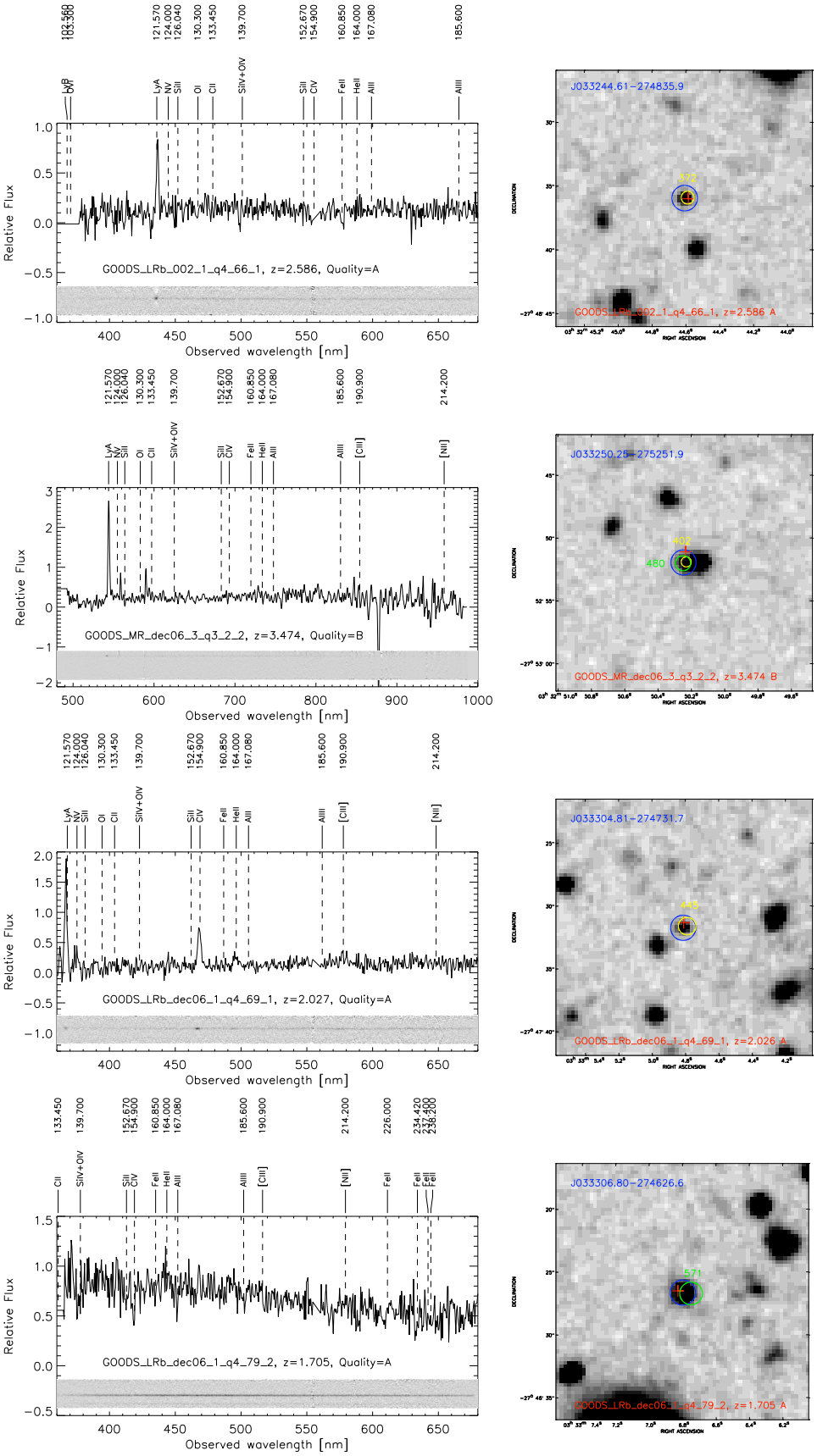

Fig. C.3. New VIMOS spectra of X-ray sources with WFI *R*-band 20″ × 20″ cutout centered on the position of the matching WFI source. Red crosses indicate the reconstructed VIMOS coordinates. The blue circles show the position of the WFI-matched objects. The yellow and green circles display the position of X-ray sources from the 2Ms CDFS or from the ECDFS catalog, respectively. Labels with corresponding colors indicate source identification numbers.